University of Glasgow

DEPARTMENT OF

AEROSPACE ENGINEERING

Development and Validation of a Discrete Vortex Method for the Prediction of Separated Incompressible Flows Around Bluff Bodies.

I. J. Taylor

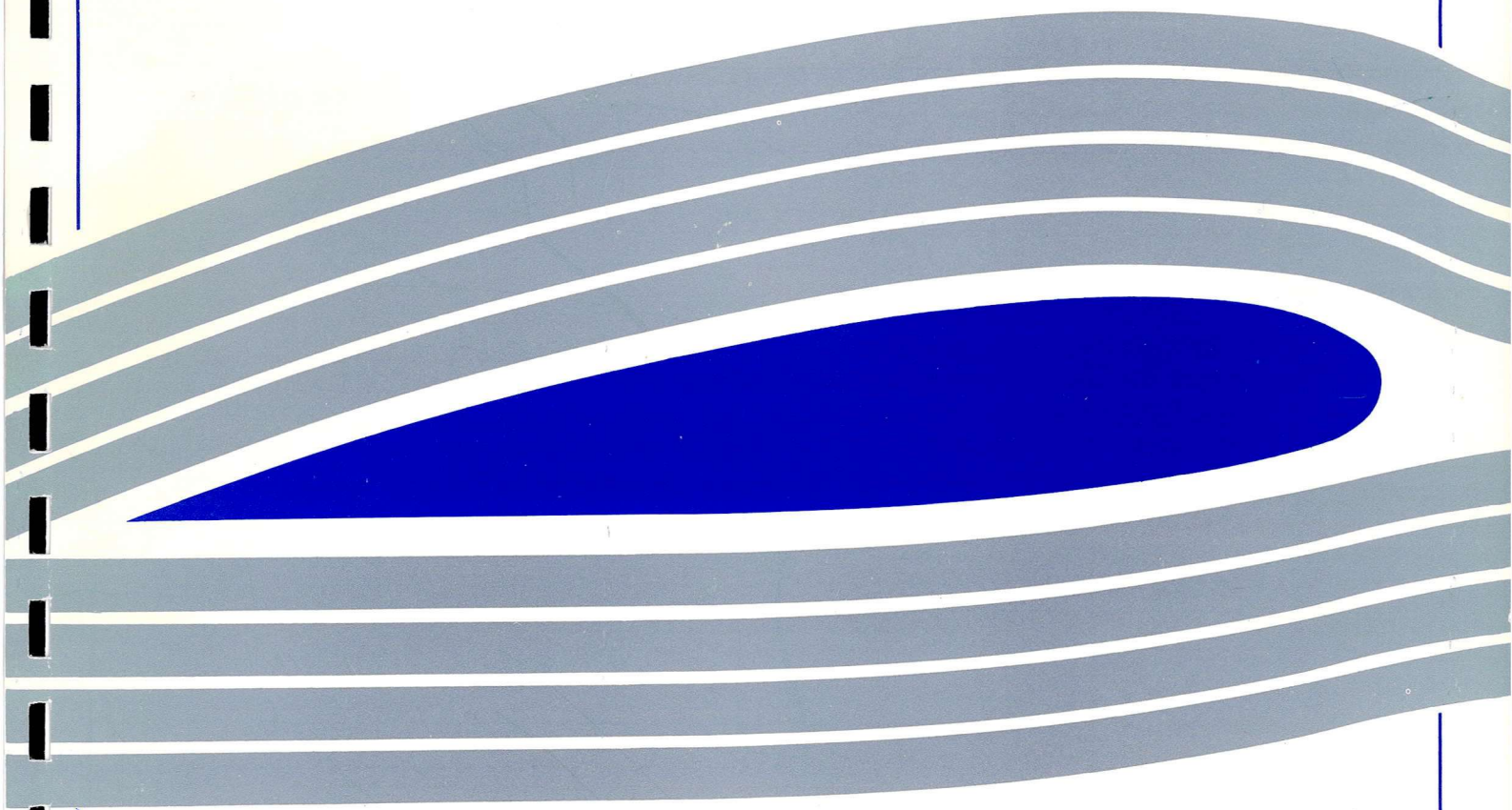

G.U. Aero Report No. 9622

Development and Validation of a Discrete Vortex Method for the Prediction of Separated Incompressible Flows Around Bluff Bodies.

I. J. Taylor

Department of Aerospace Engineering
University of Glasgow
Glasgow G12 8QQ

August 1996

SUMMARY.

A vortex method has been developed at the Department of Aerospace Engineering, University of Glasgow, for predicting separated, incompressible flow around two dimensional bodies. The method is a Lagrangian technique, with the vorticity field discretised into a series of particles, that are then tracked in the flow through time. The Biot-Savart law is used to calculate the velocity of each particle and random walks are employed to model flow diffusion. The method has successfully been validated against numerous test cases for aerofoils, however, no significant work has been carried out on validating the method for bluff body calculations, especially bodies with sharp corners.

This report presents the necessary modifications to the method, that enable reliable calculations to be made for flow fields around bluff bodies. Results of some calculations are presented against experimental data for simple bluff body geometries. Qualitatively, the results are quite encouraging, although these preliminary calculations have highlighted areas of modelling that need to be addressed in future work to improve the level of agreement with experimental data. Also presented in the report are details of a new speed up routine to improve the efficiency of the calculation.

CONTENTS.

1.0 INTRODUCTION.

1.1 Overview.

Vortex methods have undergone significant development in recent years, and are now a fairly established technique for the prediction of unsteady, incompressible flow fields. Numerous such methods now exist and can be used to analyse a wide range of applications.

The basis of vortex methods, is the discretisation of the vorticity field, rather than the velocity field, into a series of vortex particles, each with an associated vortex strength. These particles are then tracked through the flow field in time, by solving the viscous transport equation and using the Biot-Savart law to calculate the velocity of each particle. Hence, as each vortex particle is tracked in a Lagrangian manner, the necessity for a calculation grid is removed. The strength of the nascent vorticity is calculated by implementing the appropriate boundary conditions at the body surface, taking into account the influence from all areas of the flow.

Vortex methods are particularly suited to analysing unsteady and highly separated flow fields as the computations are concentrated into areas of high vorticity. This, along with the Lagrangian treatment of the particles, gives vortex methods a significant advantage over traditional Navier-Stokes solvers, where calculations are performed over the whole flow field and numerical diffusion due to the calculation grid is a common problem. Vortex methods are also well suited to analysis of moving body problems, as well as multiple body problems with bodies in relative motion. One of the main difficulties with vortex method is the computation required for the velocity calculation. The Biot-Savart law for a domain of N vortices leads to $O(N^2)$ interactions. However, reductions in the operation count can be achieved by using multipole expansions for interactions between groups of particles. A routine to implement this is described later in the report.

The vortex method is not seen as a complete replacement to more traditional CFD solvers, but is however more easily applied to a wide range of problems. Vortex methods provide a very useful and complimentary tool for the analysis of many problems in fluid mechanics.

1.2 Current Research.

A two dimensional vortex method has been developed at the Department of Aerospace Engineering, University of Glasgow, and is presented in VEZZA (1992), and LIN and

VEZZA (1994). A particular strength of this method lies in the treatment of the nascent vorticity, with the introduction of a control zone around the body to prevent spurious release or absorption of vortices. Also, the implementation of integral boundary conditions and the inclusion of curvature effects on the panel representation means that the specification of any separation points, either using a boundary layer solver or empirical data, features common in many vortex methods, are not required.

This method has been thoroughly checked and validated against a wide range of test cases for stalling aerofoils using data measured in wind tunnel tests at the Aerospace Engineering department (GALBRAITH and COTON). The results so far have been very encouraging with good agreement between predicted and measured force coefficients in a range of cases (LIN and VEZZA, 1994). However, the vortex method can potentially be used to analyse a much wider range of applications, for any general two dimensional body shape.

The motivation for the current research is to generalise the vortex method, to calculate flow fields around any general geometry, and to validate the method for bluff body calculations, especially bodies with sharp corners. Some of the required modifications to the code are presented in this report, as well of details of the development of a subroutine to speed up the vortex calculation. Also presented are results of validation of the method on simple bluff bodies compared with experimental data.

Successful validation of the method for bluff bodies can lead to a much wider range of applications for the vortex method. In particular, the method could be used to analyse more complex problems, including civil engineering applications, such as oscillating bridge deck sections. A generalised method such as this could be a very marketable analysis tool. The Lagrangian nature of the method also makes linking the calculation to a dynamic solver relatively simple. Many aeroelastic problems could then be analysed using the vortex method.

2.0 MATHEMATICAL MODEL FOR VORTEX METHOD.

The main features of the model used in the vortex method and its numerical implementation are presented in this section. A much fuller description of the methodology is given in VEZZA (1992), and LIN and VEZZA (1994).

2.1 Governing Equations.

The governing equations for two dimensional, incompressible flow, are shown below in velocity and pressure form.

Continuity : $$\nabla . \vec{\mathbf{U}} = 0 \qquad (2.1)$$

Momentum : $$\frac{D\vec{\mathbf{U}}}{Dt} = -\frac{1}{\rho}\nabla P + \nu\nabla^2\vec{\mathbf{U}} \qquad (2.2)$$

Solid region : $$\vec{\mathbf{U}}_i = \vec{\mathbf{U}}_{ic} + \vec{\Omega}_i \times (\vec{\mathbf{r}} - \vec{\mathbf{r}}_{ic}) \qquad (2.3)$$

Boundary condition : $$\vec{\mathbf{U}} = \vec{\mathbf{U}}_i \text{ on } S_i \text{ and } \vec{\mathbf{U}} = \vec{\mathbf{U}}_\infty \text{ on } S_\infty \qquad (2.4)$$

By using the definition of vorticity, $\vec{\omega} = \nabla \times \vec{\mathbf{U}}$ with $\vec{\omega} = \vec{\mathbf{k}}\omega$, and defining a vector potential $\vec{\Psi}$, such that $\vec{\mathbf{U}} = \nabla \times \vec{\Psi}$, $\vec{\Psi} = \vec{\mathbf{k}}\Psi$, $\nabla . \vec{\Psi} = 0$, then the governing equations (2.1 - 2.3) can be expressed in a vorticity and stream function form as shown below.

Continuity : $$\nabla^2\Psi = -\omega \qquad (2.5)$$

Momentum : $$\frac{D\omega}{Dt} = \nu\nabla^2\omega \qquad (2.6)$$

Solid region : $$\nabla^2\Psi_i = -2\Omega_i \qquad (2.7)$$

Boundary condition : $$\nabla\Psi = \nabla\Psi_i \text{ on } S_i \text{ and } \nabla\Psi = \nabla\Psi_\infty \text{ on } S_\infty \qquad (2.8)$$

By employing Green's second identity and implementing the boundary conditions, a solution to equation 2.4 can be obtained for the velocity field.

$$\vec{\mathbf{U}}_p = \vec{\mathbf{U}}_\infty + \frac{1}{2\pi}\int_F \omega \frac{\vec{\mathbf{k}} \times (\vec{\mathbf{r}}_p - \vec{\mathbf{r}})}{\left\|\vec{\mathbf{r}}_p - \vec{\mathbf{r}}\right\|^2} dF_b + \frac{1}{2\pi}\int_{S_i} 2\Omega_i \frac{\vec{\mathbf{k}} \times (\vec{\mathbf{r}}_p - \vec{\mathbf{r}})}{\left\|\vec{\mathbf{r}}_p - \vec{\mathbf{r}}\right\|^2} dS_i \qquad (2.9)$$

This is analogous to the Biot-Savart law in electromagnetism, for the magnetic field induced at a point. In the vortex method, the velocity at a point is calculated by considering the influence of all areas of the flow. The RHS represents the influence of the free stream, the vorticity in the flow field (split into the vorticity in the control zone close to the body, and vorticity in the remainder of the flow), and the vorticity inside the body, due to rotational motion of the body.

2.2 Panel Representation and Discretisation of Vorticity.

The two dimensional body is defined by a series of nodes, which lie on the surface of the body. Adjacent nodes are connected by straight lines, forming a series of panels, giving a polygonal representation of the body surface. Each panel is further divided forming a series of sub-panels (Fig. 2.1).

A small distance away from the body surface, a control zone is set up, in which the vorticity is created. This nascent vorticity in the control zone, is discretised using a panel technique. The distribution of nascent vorticity is represented by a series of vortices, with one at each node on the body surface. The vorticity is then assumed to vary linearly between adjacent nodes along each panel (Fig. 2.2). The distribution is then further broken down, such that a series of vortex "blobs" can be created, with one for each sub-panel. These particles are created a small distance away from the wall, δ, which will depend on Reynolds number and surface roughness. This then provides the distribution of nascent vorticity that can be convected and diffused and hence giving rise to vorticity in the remainder of the flow field.

The boundary condition (2.8) is implementing by ensuring zero mass flow across each panel on the body surface. The condition is implemented such that there is no normal velocity component at the nodes, although this does not guarantee that condition (2.8) will be fulfilled at every point on the panel. When considering the normal velocity component at each node, the contribution to the mass flow from all of the different sources must be taken into account. The implementation of the boundary condition (2.8) can be expressed as

$$F_{jf} + F_{jv} + F_{jn} + F_{js} + F_{ji} = 0 \qquad (2.10)$$

with each term representing a contribution to the normal velocity component at each node. The first three terms represent the contribution from the free stream, the vortices outside the control zone (wake vortices) and the nascent vorticity inside the control zone respectively. The last two terms arise from the motion of the body, with the first giving

the contribution from the surface velocity (both linear and rotational) and the second from the vorticity inside the body due to rotational motion. The derivation of each of these terms is given in more detail in LIN and VEZZA (1994).

Accounting for all these terms leads to a system of *N* equations that can be solved to give the strength, γ, of the nascent vortices at the *N* surface nodes. However, only *N-1* panels are required to satisfy the zero mass flow condition, as the mass flow for the final panel will automatically be zero, as there is no source or sink in the body. A further condition is required to make the solution unique and is obtained from Kelvin's theorem. The circulation of the flow field remains constant as there are no external sources of vorticity. Hence, additional condition is

$$\sum_i \Gamma_i + \sum_{m=1}^{N} \sum_{k=1}^{K} (\Gamma_m)_k + \Gamma_{st} + 2\Omega_i A_i = 0 \qquad (2.11)$$

2.3 Convection and Diffusion.

The vorticity transport equation (2.6) can be written as

$$\frac{\partial \omega}{\partial t} + (\vec{U}.\nabla)\omega = \nu\nabla^2\omega \qquad (2.12)$$

The solution of this non-linear equation is very difficult and so is solved by a two stage process. This method of operator splitting first gives a governing equation for the convective term (2.13) and secondly, the diffusive term (2.14)

Convection : $$\frac{\partial \omega}{\partial t} + (\vec{U}.\nabla)\omega = 0 \qquad (2.13)$$

Diffusion : $$\frac{\partial \omega}{\partial t} = \nu\nabla^2\omega \qquad (2.14)$$

The convective term is solved exactly for point vortices, as the velocity of each vortex particle, is given by the velocity at the particle location. When vortex blobs are employed, the velocity of the centre of the particle is used, although this only provides an approximation to the solution. The new position of the centre of a vortex after time $t+\Delta t$, due to convection is

$$(z_i(t+\Delta t))_c = z_i(t) + V_i(t).\Delta t \qquad (2.15)$$

The diffusion equation (2.14) can be solved to give

$$\omega = \frac{1}{4\pi\nu\Delta t} e^{-\frac{r^2}{4\nu\Delta t}} = \frac{1}{4\pi\nu\Delta t} e^{-\frac{(x^2+y^2)}{4\nu\Delta t}} \qquad (2.16)$$

which is equivalent to a probability density function for a Gaussian distribution, with mean equal to zero and standard deviation equal to $\sqrt{(2\nu\Delta t)}$. From this, the diffusion of vorticity in the flow field can be modelled by a Random walk (CHORIN, 1973). For each vortex, two random numbers η_x and η_y are generated from the Gaussian distribution $(0,\sqrt{(2\nu\Delta t)})$, so that (η_x,η_y) represents the change in position of the vortex due to diffusion. Combining the convection and diffusion is done by simply adding the convective and diffusive increments to the position of the vortex at time t, to obtain the position at time $t+\Delta t$.

$$(z_i(t+\Delta t))_c = z_i(t) + V_i(t).\Delta t + (\eta_x + i\eta_y) \qquad (2.17).$$

2.4 Release and Absorption of Vortices.

The control zone is set up around the body, to ensure that an excessive number of vortices are not released into the flow field to ensure that the boundary conditions are implemented in a stable manner. This also helps to minimise the computational operation count for the velocity calculation. After a nascent vortex has been convected and diffused, it is released into the wake if it has crossed the control zone boundary, otherwise it is absorbed (Fig. 2.3). Vortices already in the wake are also absorbed, if they cross the control zone boundary. All the absorbed vortices are then replaced by nascent vortices, which also include the newly created vorticity for the next time step, at the nascent vortex positions on each sub-panel.

The implementation of the control zone has ensured that nascent vortices are not spuriously released into the wake. Also, as the zero mass flow condition is only implemented at discrete points along the surface, there will be some leakage across the panel, although there should be a balance between inflow and outflow. However, this will have an effect on the local velocity of the nascent vortices. For this reason, the border of the control zone is set further from the wall than the position of the nascent vortices to prevent any premature vortex release (Fig. 2.3). As a consequence, it has been found that no separation points need defining in the calculation, either through

empirical correlations or from a boundary layer solver, which are common features of many other vortex methods.

It should also be noted that for an accurate discretisation of the nascent vorticity, the vortices on each subpanel should overlap (Fig. 2.4). This also helps to reduce the local velocity perturbations and leakage across each panel, that arise from the discretisation of the vorticity field and the implementation of the boundary conditions. These factors point towards a more accurate solution with more, overlapping vortices. However, as the calculation operation count is of $O(N^2)$, then care must be taken to achieve a balance between obtaining an accurate solution and keeping the required CPU down to a practical level.

2.5 Vortex Merging.

One of the main disadvantages with vortex methods is the large amount of computational cost that is associated with large numbers of particles. The velocity calculation involves $O(N^2)$ interactions in a flow field with N particles. For this reason, for the method to be practical, there needs to be a means for making sure that the number of particles in the flow field does not get excessively large.

One method to achieve this is to merge two particles into a single particle. Two vortices may be merged, provided that they are a large distance from the body, are not a great distance apart and are not of similar strength but opposite sign (SPALART, LEONARD and BAGANOFF, 1983). However, the resulting particle is only an approximation for the previous two particles and as such an error is introduced into the calculation. Vortices are therefore only combined provided that the new particle introduces an error smaller than some predetermined error limit. It should also be noted that this merging process is irreversible.

Assuming two vortices are located at positions Z_1 and Z_2, with strengths Γ_1 and Γ_2 respectively, then they can be merged into a single vortex at Z with strength Γ, where the position of the new particle is given by

$$Z = \frac{\Gamma_1 Z_1 + \Gamma_2 Z_2}{\Gamma_1 + \Gamma_2} \tag{2.18}$$

and it's circulation is given by,

$$\Gamma = \Gamma_1 + \Gamma_2 \tag{2.19}$$

The error in the induced velocity for the new particle at Z, can be calculated from the LHS of (2.20). The merging procedure only takes place provided that the error is less than some predetermined limit.

$$\frac{|\Gamma_1\Gamma_2|}{|\Gamma_1+\Gamma_2|}\cdot\frac{|Z_1-Z_2|^2}{(D_0+d_1)^{1.5}(D_0+d_2)^{1.5}}\leq V_0 \qquad (2.20)$$

where d_1 and d_2 are the distances from the body to the two respective particles, V_0 is the velocity tolerance (error) and D_0 is a distance parameter. It is clear from (2.20) that vortices are more likely to be merged if they are close together, have small strength of similar sign and are a long distance from the body. However, care must be taken as merging when the above criteria has been satisfied, is not always appropriate. Vortices that are sufficiently far from the body may be merged, but later in the calculation may move back towards the surface later in the calculation. For example, in the wake of a bluff body where the large vortical structures lead to significant recirculation back towards the body. In this case, the merged vortex may have a significantly different influence on the flow structure than the two separate particles might have. A simple solution is to have a varying tolerance V_0, small for particles close to the body, and larger in the far wake where the flow field has less influence. However, as discussed above, for bluff body calculations, care must be taken as to what can be termed the "far wake", and in this case, a more complex solution may be required.

3.0 GENERALISATION OF MODEL.

As mentioned in section 1.2, the vortex method has been validated successfully on a number of aerofoil test cases. However, this validation has resulted in a number of aspects of the modelling being set up specifically for aerofoil type geometries. For the vortex method to run successfully on more general geometries, such as bluff bodies, the modelling has to be modified to be able to handle a much wider range of test cases. This section outlines some of the modifications that have been made to generalise the model.

3.1 Improvement of Vortex Absorption.

For each vortex, there is a check to find if it remains in the wake, or is absorbed into the control zone. To carry out this check, the distance between the vortex of interest and the

nearest point on the body surface needs to be found and is calculated using the following procedure.

Firstly, the nearest node point on the body surface to the vortex is found. Then it is ascertained if the particle is either upstream or downstream of the node point (Fig. 3.1). If it is upstream, then the distance of the particle from the upstream panel, in the direction normal to that panel is found. Similarly, if the particle is downstream, the distance normal to the downstream panel is found. If the normal distance that is found is less than the thickness of the control zone, then the particle will be absorbed (Fig. 3.1)

This procedure works very well for aerofoil type geometries where the angle between adjacent panels is not very large. However, for bluff bodies with sharp corners, this can lead to vortices being incorrectly absorbed, as shown in Fig. 3.2.

The particle at *P*, is clearly nearest the node *N* on the body surface. As the particle is downstream of the node, the normal distance to panel *n-1* is used in the absorption check rather than the distance to panel *n*. Clearly the particle is outside the control zone, but as the distance to panel *n-1* is less than the control zone thickness, the particle is incorrectly absorbed. When the two panels are nearly perpendicular to each other, this can clearly lead to particles a large distance from the body being absorbed.

The problem has been removed by introducing a further check into the absorption criteria. If a particle is nearest to node *N*, and the normal distance is being checked relative to the downstream panel, *n-1*, then the distance of the particle from the previous node *N-1* is also checked (Fig. 3.3).

If the particle is a distance greater than the length of panel *n-1* and the control zone thickness, then the particle will not be absorbed. The effect of this is to join the control zones above the two neighbouring panels smoothly (Fig. 3.3), thus removing the discontinuity between the panels that previously existed (Fig. 3.2).

3.2 Improvement of Vortex Merging.

As part of the calculation to check if two particles can be merged, the distance of each particle to the nearest point on the body surface is required. For aerofoil geometries, to save computational effort, it could be assumed that for particles upstream of the body, the required distance would just be the distance to the leading edge of the aerofoil (Fig. 3.4a). Similarly, for particles downstream, the distance to the trailing edge is used.

However, when calculating about bluff bodies such as rectangles, with large front and rear faces, one cannot make this assumption. If the middle of the rear face is assumed to be the "trailing edge" of the body, then vortices near the corners of the body, are a long way from this point and may in fact be merged even though they are close to the body (Fig. 3.4b).

For this reason, the calculation was modified to find the distance to the nearest point on the body surface for every vortex particle, rather than assume a nearest point as discussed above. This does lead to a little more computational effort on each timestep, but for bluff body calculations, particularly rectangular geometries, this has been seen to be a necessary modification.

3.2 Body Definition for Regions of High Curvature.

Each panel is created by joining two adjacent nodes with a straight line and the sub-panels are then formed by dividing the panel up equally as shown in Fig. 2.2. The nascent vorticity is then discretised into blobs on each sub-panel as discussed in section 2.2. This provides a good approximation to the body geometry in regions where the surface curvature is low. However, for high curvature regions, extra definition is required to model the body correctly (LIN and VEZZA, 1994). The node positions are again given, but in this case the co-ordinates of the sub-panel nodes are also given. This allows the curvature between two adjacent nodes to be modelled reasonably simply and more accurately. The nascent vorticity is again discretised on each sub-panel in the same manner (Fig. 3.5).

The position of the nascent vortices for regions of low surface curvature, can be approximated by

$$(z_m)_k = \left[\left(\frac{K-k+\frac{1}{2}}{K}\right)Z_m + \left(\frac{k-\frac{1}{2}}{K}\right)Z_{m+1}\right] - i\frac{Z_{m+1}-Z_m}{|Z_{m+1}-Z_m|}\delta \qquad (3.1)$$

which is equivalent to a straight panel with K equally spaced vortices as shown in Fig. 2.2. For high curvature regions the position of a nascent vortex above the kth sub-panel on panel m is given by

$$(z_m)_k = \frac{1}{2}((Z_m)_{k+1} + (Z_m)_k) - i\frac{(Z_m)_{k+1} - (Z_m)_k}{|(Z_m)_{k+1} - (Z_m)_k|}\delta \tag{3.2}$$

In the current vortex method, only one region of high curvature definition can be used in the calculation. For aerofoil cases, this is adequate as the extra definition is only really required around the leading edge. However, for more general body geometries, there may well be cases where the high definition is required in a number of locations on the body surface. For this reason the code has been modified to allow any number of regions of high curvature definition.

3.3 General Body Motion.

Another advantage of the Lagrangian nature of the vortex method, is the ability to calculate the flow field about moving bodies relatively simply. For the aerofoil test cases, the body motion is generally either rotational or a constant linear velocity in one direction. The model has been set up for both of these conditions, however, other types of body motion may be required for different applications.

The linear velocity model has now been extended to allow a sinusoidal type body velocity one or both of the x and y directions. Also, it is anticipated that in the near future, a much more general linear velocity may be implemented. In this case, the velocity profile will be entered as a time history from an input dataset, which would allow an almost random velocity profile to be entered. Potential then exists for extending this further, by linking this dataset to a dynamic solver, so that aeroelastic effects could be modelled.

4.0 VELOCITY CALCULATION SPEED UP USING ZONAL DECOMPOSITION.

In this section, techniques aimed at improving the efficiency of the algorithm are presented. Firstly, a brief review of recent research is given, highlighting some of the various methods that may be used. The zonal decomposition / multipole expansion method incorporated into the vortex method is then discussed, showing the improvement that has been made in the efficiency of the calculation and how this may be further improved.

4.1 Summary of Recent Research.

In calculating the velocity at a point in the flow field, the influence of all the vorticity must be taken into account. This involves a calculation of $O(N^2)$ interactions for a flow field made up of N particles, which can lead to a large computational cost. A number ways of reducing the number of interactions in this calculation have been reported by a various researchers.

One technique is the Vortex-in-Cell (VIC) method. A fixed mesh of M nodes is fitted over the domain of the flow field. The vorticity is still treated in a Lagrangian manner, but is interpolated onto the mesh. The continuity equation is then solved for the stream function at each node in the mesh. Differentiation gives the velocity, which can then be interpolated back from the mesh to each vortex location. The VIC method is described in more detail in LEONARD (1980) and SMITH and STANSBY (1988). The operation count for a flow field of N vortex particles is $O(N+M\log M)$, a significant improvement on the straightforward direct summation technique.

The main drawback of the VIC method is that some of advantages of the vortex method are lost with the need to fit a Eulerian mesh to the flow field. The interpolation to and from the mesh will include areas of the flow where there is little or no vorticity. Also, the interpolations will introduce a little numerical diffusion. LEONARD (1980) reports that researchers have found that "numerical experiments ... indicate that although these fine scale errors are present they may not seriously affect the large-scale features." SMITH and STANSBY (1988) report good results using the VIC method on a circular cylinder, although claim that for an accurate calculation, a large number of particles is required.

A more popular speed up technique is the so called Multipole Expansion or Zonal Decomposition method. This method has been implemented by a number of researchers in slightly different guises. The basic philosophy is to decompose the flow field into a series of zones. Provided that a zone is sufficiently far from the point of interest, then the contribution of the particles in the zone to the velocity calculation, can be found by a Laurent series expansion rather than from direct summation of all the particles. The advantages of this technique are that the Lagrangian nature of the vortex method is retained and accurate results can be obtained with a significant reduction in the operation count. Both CLARKE and TUTTY (1994), and VAN DOMMELEN and RUNDENSTEINER (1989) claim an operation count of $O(N\log_2 N)$ for a flow field of N particles, whereas GREENGARD and ROKHLIN (1987) claim $O(N)$.

GREENGARD and ROKHLIN (1987) start with an initial square zone that contains the whole flow field. At each level, every zone is divided into four smaller square zones, until the required precision is reached at level l. Hence, at level l there will be 4^l distinct zones. For each zone i, a neighbourhood is established, which consists of all zones adjacent to i. For these zones the velocity influence is found using direct summation. For zones not in the neighbourhood of i, but within the neighbourhood of i's parent zone, the velocity influence of zone i is found from the series expansion (Fig. 4.1). As the algorithm requires a single pass through all the zones, starting with the largest zones, the influence of a zone (and the vortex particles it contains) on every other zone is taken into account. A parallel version of this algorithm has been reported by GREENGARD and GROPP (1990) claiming a further reduction in the operation count to $O(N/p+\log p)$ where p is the number of processors.

As the zonal decomposition is performed uniformly over the whole flow domain, the algorithm performs most efficiently when the distribution of particles is uniform. This is not the case in most applications of the vortex method. Both VAN DOMMELEN and RUNDENSTEINER (1989), and CARRIER, GREENGARD and ROKHLIN (1988) report an "adaptive" algorithm which allows more efficient calculation for none uniform distributions of particles. In this case, the initial zone is split into four smaller zones, as in GREENGARD and ROKHLIN (1987). Further subdivision of each panel is only made if the panel contains greater than a specified number of vortex particles (Fig. 4.3). The zonal contribution of each zone to the velocity calculation is then performed in much the same way as described above.

CLARKE and TUTTY (1994) use a similar method, although the zonal decomposition is performed using rectangular rather than square cells. The initial zone is set up to contain the entire flow field. This zone is then split into two smaller zones, along the longest dimension, such that half the particles are contained in each of the new sub-panels. The decomposition continues in a similar manner until each zone contains a minimum number of particles. The velocity calculation is then performed in a similar manner to GREENGARD and ROKHLIN (1987), although the influence of a zone on the velocity at a point in the flow field seems to be considered, rather than the influence of a zone on other zones as discussed previously. This may lead to a higher operation count than the $O(N\log N)$ that is claimed, although a significant speed up from the direct summation method is reported.

The advantage of the zonal decomposition used in CLARKE and TUTTY (1994), is that dividing the zones such that half the particles are in each sub-panel ensures an even distribution of particles in each zone. The other methods often lead to some zones

containing very few particles, which can mean that some of the savings in the operation count are lost. Calculating the series expansion for a zone with few particles, can be as expensive as using direct summation for the velocity calculation. The rectangular zones however, can lead to zones with quite a high aspect ratio. This may result in the velocity influence at points far from the zone, being calculated from direct summation when a series expansion would have been sufficient.

4.2 Implementation of Zonal Decomposition in the Vortex Method.

A zonal decomposition technique based on the research discussed above, has been implemented in the vortex calculation. A square "adaptive" zonal decomposition similar to VAN DOMMELEN and RUNDENSTEINER (1989) is employed, but with a less sophisticated numbering system. The whole computational flow field is initially contained in a single square zone. This is then divided into four sub-panels. Each panel is then further subdivided into four new zones, provided that there is a minimum number of particles in the zone, thus creating a hierarchical structure of zones (Fig. 4.3). For each panel, the parent zone, and any children (sub-panels) of the zone are recorded, along with which particles are stored in that zone.

For each vortex particle, Z_j, the distance to the centre of a zone, Z_c, is compared with the radius of a zone, λ, where the radius is half the length of the side of the panel. Where the particle is a distance from Z_c,greater than some factor times λ, then the Laurent series will converge, and the contribution to the velocity at Z_j from the zone can be calculated from zonal expansion (Fig. 4.2). The children of this zone are then ignored, as all the particles in this zone have been taken into account. If the particle is too close to Z_c for the series to converge, then the zones children are considered in the same way. This process continues until the zonal expansion can be used, or the smallest zone is reached, and if the series will still not converge, the velocity contribution is calculated from direct summation. The hierarchical structure to the algorithm means that the largest possible zone is used at all times. This technique is similar to that discussed in CLARKE and TUTTY (1994), for calculating the influence of all the zones on the velocity at a point.

The contribution of a zone to the velocity at a point Z, can be calculated from a series expansion using the following,

$$U(z) - iV(z) = \sum_k \frac{\alpha_k}{2\pi i (z - Z_c)^k} \qquad : k=1,N_t \qquad (3.3)$$

where

$$\alpha_k = \sum_j \Gamma_j (Z_j - Z_c)^{k-1} \qquad : j=1,N_p \; ; \; k=1,N_t \qquad (3.4)$$

and where, α_k are the coefficients of the series expansion. Z_c is the centre of the zone and there are N_p particles contained in the zone.

The implementation of this routine has resulted in an reduction in the CPU required for the velocity calculation of the order of 35% and a reduction of around 30% for the whole timestep. Although this improvement is significant, it is not as much as was hoped for when comparing a reduction in the operation count from $O(N^2)$ to $O(N\log N)$. A comparison of CPU for the velocity calculation against number of vortices shows the improvement that has been made, although the relationship between the CPU and N is still not linear (Fig. 4.4).

The method that has been implemented finds the velocity influence of each zone on each particle, whereas the methods described above find the influence of each zone on other zones. It is clear that further improvement in the efficiency of the algorithm is possible and it is intended that a multipole expansion technique similar to that presented in VAN DOMMELEN and RUNDENSTEINER (1989) will be implemented in the near future.

5.0 BLUFF BODY CALCULATIONS AND VALIDATION.

A generalised vortex method could be used to analyse complex geometries, and could be applied to such problems as oscillating bridge deck sections. However, before these cases can be investigated, the method needs to be validated on simple bluff body geometries, to give confidence in any predictions that are obtained. The following section describes this validation and compares the results with experimental data. The validation was performed on two simple geometries, a square and a circle, for which numerous published experimental results exist. It should be noted that all the bluff body calculations were performed prior to the incorporation of the multipole expansion technique described in section 4.2.

5.1 Bluff Body Models.

The square calculations were performed at a range of different angles incidence to the oncoming free stream flow. Each calculation was at a Reynolds number of 34000.

These calculations did not match experimental conditions exactly, but fell within a range of conditions covered in experimental results from VICKERY (1966), LEE (1975) and OBASAJU (1983). The comparison is valid, as the vortex shedding frequency (Strouhal number) does not vary greatly with Reynolds number (OBASAJU, 1983) as shown in Fig. 5.1). The body geometry was formed using 160 panels, each with 5 sub-panels (nascent vortices). The side length of the square was 1, with the core radius of the vortex particles and the creation distance from the wall set to 0.005.

Much less validation was performed on the circle, due to the results that were obtained on the square model. The model was set up with a Reynolds number of around 6×10^5. The body geometry was formed using 150 panels, each with 5 sub-panels. It was felt that this definition was fine enough for the high curvature definition option not to be used. The diameter of the circle was 1, with the core radius of the vortex particles and the creation distance from the wall set to 0.0025.

5.2 Results

5.2.1 Square Body Calculation.

Calculations were performed on the square body at a range of incidence to the flow, starring at 0° up to 20°, at 5° intervals. The lift and drag coefficients for the 0° and 15° cases are shown in Fig. 5.2 and 5.3 respectively. The direction of the two force coefficients are calculated in directions perpendicular and parallel to the direction of the free stream velocity. Snapshots from the flow field for these two cases are shown in Fig. 5.4 and 5.5.

The vortex shedding frequency can be non-dimensionalised, to give the Strouhal number from

$$St = \frac{nd}{\mathrm{U}} \qquad (5.1)$$

where, U is the free stream velocity, n is the vortex shedding frequency and d is the side length of the body.

For the 0° case, the lift plot shows the flow field settling down into a fairly regular pattern of vortex shedding. As expected, due to the symmetrical nature of the calculation, the mean lift coefficient is around zero. However, there appears to be two parts to the vortex shedding, which can be seen in the lift plot (Fig. 5.2), with a smaller

oscillation superimposed onto the main oscillation. The most dominant shedding (larger amplitude with lower frequency) corresponds to vortex shedding from the two side faces (parallel to the free stream) and the smaller part corresponds to shedding from the rear face of the body. This phenomena is not reported in any of the experimental results. The 15° case has a much more regular pattern, with vortex shedding occurring of the upper side face only.

An estimate of the Strouhal numbers for the vortex shedding in the numerical predictions can be obtained from a Fast Fourier Transform (FFT) of the lift coefficient. The Strouhal numbers in the 0° case are 0.065 for the main vortex shedding and 0.2 for the smaller shedding. Experimental results for the 0° case, also obtained from FFT, give a Strouhal number of 0.13. The variation of Strouhal number with angle of incidence is compared with various experimental data in Fig. (5.6). The variation of the mean drag coefficient is also compared with experimental data in Fig. (5.7). It is clear that although the flow field qualitatively looks quite reasonable, quantitatively, the numerical predictions are far from adequate.

The mean pressure distribution around the body, shows quite a good agreement with experimental data on the front and rear faces, but is less accurate on the side faces (Fig. 5.8). This discrepancy is not yet fully understood, but may be caused by the vortices being reabsorbed into the control zone. With the significant recirculation in the wake, a large number of vortices may be reabsorbed on each timestep. When the nascent vorticity is then rediscretised, some of the new vortex strengths may be quite high due to the large amount of reabsorbed vorticity. It has also been observed that the vortices that are shed from the body tend to be of quite high strength, leading to quite large "pulses" in the pressure distribution. A combination of these factors may explain the differences observed in the pressure distribution and may also be a symptom of the discrepancies in the vortex shedding predictions.

The results for the aerofoil predictions did show a tendency for a lack of diffusion in the solution. However, this was not a major problem as it was most noticeable in the large vortices that were moving away from the body. For bluff body cases, the large separated wakes, with significant recirculation of vortices back towards the body, this lack of diffusion may become significant. It is felt that this may be the main cause of the disappointing predictions for bluff bodies. The random walk technique only really models laminar diffusion, and thus lends weight to the above argument. Clearly, some form of modelling for the turbulent diffusion may be required in the method. An investigation into how this can be implemented will take place in the near future.

5.2.2 Circular Body Calculation.

The lift and drag for the circle and snapshots from the flow field are shown in Fig. 5.9. A very clear vortex shedding pattern can be seen in this solution, giving a Strouhal number of 0.375 compared with a value of 0.21, derived from experimental data at this Reynolds number. The vortices in the wake can be seen to be very dense and tightly packed, with very little diffusion (Fig. 5.10). The high Reynolds number for this calculation, means that the diffusive term from the random walk is very small. Again it is clear that a way of modelling the turbulent diffusion may be needed in the vortex method for accurate predictions of bluff body flows.

Another problem that was encountered in this model was the sensitivity of the calculation to the creation distance of the nascent vortices from the wall. The circle model was initially set up with the creation distance and vortex core size set to 0.005. However, this resulted in a very thin wake with the separation points very close to the rear edge of the body. Changing the creation distance and core size to 0.0025, gave the solution discussed here. A small change in the parameters gave a vastly different solution, demonstrating a strong sensitivity. These parameters were not varied for the square body and may not yet be optimised. Future work will try to reduce the sensitivity of these parameters and also to incorporate some method of automatic optimisation.

6.0 CONCLUSIONS.

A vortex method has been developed at the Department of Aerospace Engineering, University of Glasgow, and validated on aerofoil test cases. The method has now been modified to calculate the flow field around bluff body geometries.

Initial results for simple bluff body geometries are qualitatively quite encouraging, although quantitatively a little disappointing. It is felt that improved modelling of the diffusion terms, to include turbulent diffusion as well as laminar diffusion may be required. An investigation into how this modelling should be incorporated will be carried out in the near future. The way in which vorticity is reabsorbed into the control zone may also require some modifications.

A zonal decomposition / multipole expansion speed up technique has been incorporated into the method. This has given a reduction of around 30% in the CPU required for the

velocity calculation. A much greater improvement is anticipated with further modifications to the multipole expansion algorithm.

Once the vortex method has been validated for simple bluff bodies, the method could be used to analyse a much wider range of applications, such as Civil Engineering problems, including oscillating bridge deck sections.

NOMENCLATURE.

A	Area of body section.
d	Distance of particle from body surface.
d	Characteristic body dimension.
F	Flow field.
k	Index number for subpanel.
K	Number of subpanels on panel.
$\vec{\mathbf{k}}$	Unit vector.
n	Vortex shedding frequency.
N	Number of vortices in flow field.
N	Number of body panels.
P	Pressure.
r	Magnitude of position vector.
$\vec{\mathbf{r}}$	Position vector.
St	Strouhal number.
S	Body surface.
t	Time.
U,V	Velocity.
$\vec{\mathbf{U}}$	Velocity vector.
Z,z	Complex position of vortex particle.
α	Coefficients for series expansion.
γ	Circulation density for vortex particle.
Γ	Circulation.
δ	Creation distance for nascent vorticity.
η	Random variable for diffusion modelling.
ν	Viscosity.
ρ	Fluid density.
$\vec{\Psi}$	Vector potential.
Ψ	Stream function.

$\vec{\Omega}$ Rotational velocity vector.

ω Vorticity.

$\frac{D}{Dt}$ Lagrangian / material derivative.

∇ Gradient operator.

∇^2 Laplace operator.

$\nabla \times$ Curl.

$\nabla .$ Divergence.

Subscripts.

c Reference point (centre) for body motion.

f Free stream.

i Index number for solid body.

i Index number for vortex particles outside control zone.

i Equivalent vorticity inside body.

j Index number for panel.

k Index number for subpanel.

k Index number for terms in series expansion.

m Index number for panel.

n Nascent vorticity.

p Point in flow field.

s Surface of body.

st Starting condition.

v Vorticity outside control zone.

∞ Far field.

REFERENCES.

BEARMAN, P.W. and OBASAJU, E.D., 1982, "An Experimental Study of Pressure Fluctuations on Fixed and Oscillating Square-Section Cylinders." Journal of Fluid Mechanics, Vol. 119, pp. 297-321.

CARRIER, J., GREENGARD, L. and ROKHLIN, V., 1988, "A Fast Adaptive Multipole Algorithm for Particle Simulations." SIAM Jl Sci. Stat Comput, Vol. 9, pp. 669-686.

CHORIN, A.J., 1973, "Numerical Study of Slightly Viscous Flow." Journal of Fluid Mechanics, Vol. 57, pp. 785-796.

CLARKE, N.R. and TUTTY, O.R., 1994, "Construction and Validation of a Discrete Vortex Method for the Two-Dimensional Incompressible Navier-Stokes Equations." Computers Fluids, Vol. 23, No. 6, pp. 751-783.

GALBRAITH, R.A.McD. and COTON, F.N., "A Review of Low Reynolds Number Aerodynamic Research at the University of Glasgow".

GREENGARD, L. and GROPP, W.D., 1990, "A Parallel Version of the Fast Multipole Method." Computers Math. Applic., Vol. 20, No. 7, pp. 63-71.

GREENGARD, L. and ROKHLIN, V., 1987, "A Fast Algorithm for Particle Simulations." Journal of Computational Physics, Vol. 73, pp. 325-348.

LEE, B.E., 1975, "The Effect of Turbulence on the Surface Pressure Field of a Square Prism." Journal of Fluid Mechanics, Vol. 69, Part 2, pp. 263-282.

LEONARD, A., 1980, "Vortex Methods for Flow Simulation." Journal of Computational Physics, Vol. 37, pp. 289-335.

LIN, H and VEZZA M, 1994 "Implementation of a Vortex Method for the Prediction of Separated Incompressible Flows." G.U. Aero Report No. 9425

OBASAJU, E.D., 1983, "An Investigation of the Effects of Incidence on the Flow Around a Square Section Cylinder." Aeronautical Quarterly, Vol. 34, pp. 243-259.

SARPKAYA, T., 1989, "Computational Methods with Vortices - The 1988 Freeman Scholar Lecture." Journal of Fluids Engineering, Vol. 111, pp. 5-52.

SARPKAYA, T. and IHRIG, C.J., 1986, "Impulsively Started Steady Flow About Rectangular Prisms : Experiments and Discrete Vortex Analysis." Journal of Fluids Engineering, Vol. 108, pp. 47-54.

SMITH, P.A. and STANSBY, P.K., 1988, "Impulsively Started Flow Around a Circular Cylinder by the Vortex Method." Journal of Fluid Mechanics, Vol. 194, pp. 45-77.

SPALART, P.R., LEONARD, A. and BAGANOFF, D., 1983, "Numerical Simulation of Separated Flows." NASA TM 84328.

VAN DOMMELEN, L. and RUNDENSTEINER, E.A., 1989, "Fast, Adaptive Summation of Point Forces in the Two-Dimensional Poisson Equation." Journal of Computational Physics, Vol. 83, pp. 126-147.

VEZZA, M., 1992, "A New Vortex Method for Modelling Two-Dimensional, Unsteady Incompressible, Viscous Flows." G.U. Aero Report No. 9245.

VICKERY, B.J., 1966, "Fluctuating Lift and Drag on a Long Cylinder of Square Cross-Section in a Smooth and in a Turbulent Stream." Journal of Fluid Mechanics, Vol. 25, Part 3, pp. 481-494.

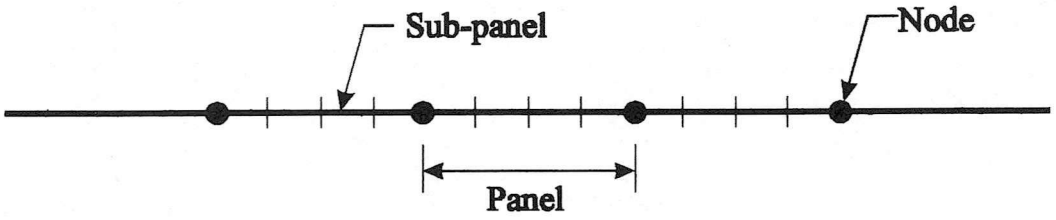

Fig. 2.1 - Body Surface Definition.

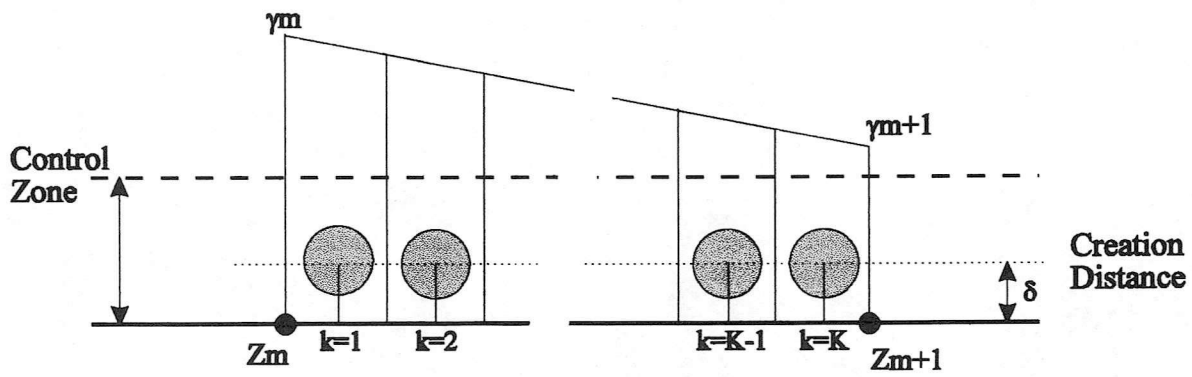

Fig. 2.2 - Discretisation of Nascent Vorticity.

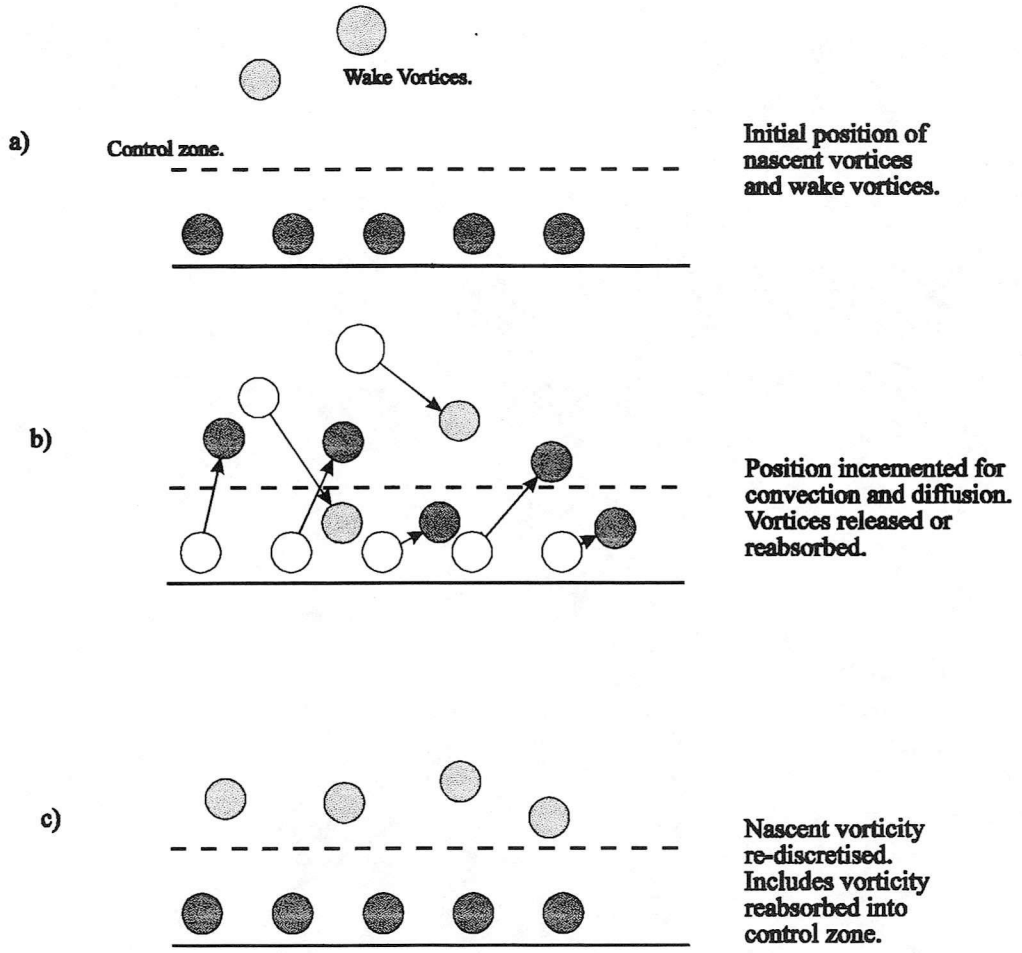

Fig. 2.3 - Vortex Release and Absorption.

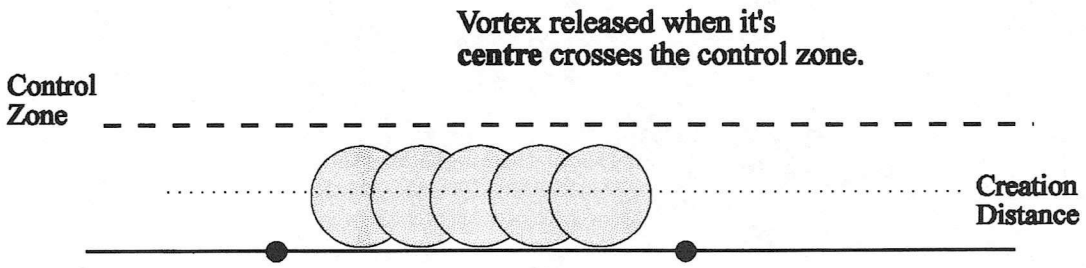

Fig. 2.4 - Control Zone Position.

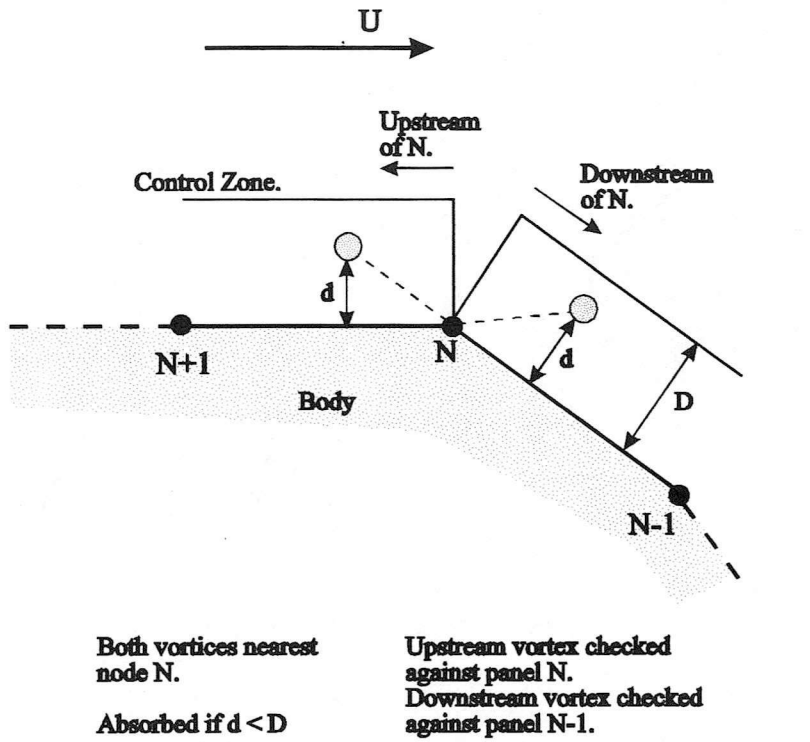

Fig. 3.1 - Method of Checking for Vortex Absorption.

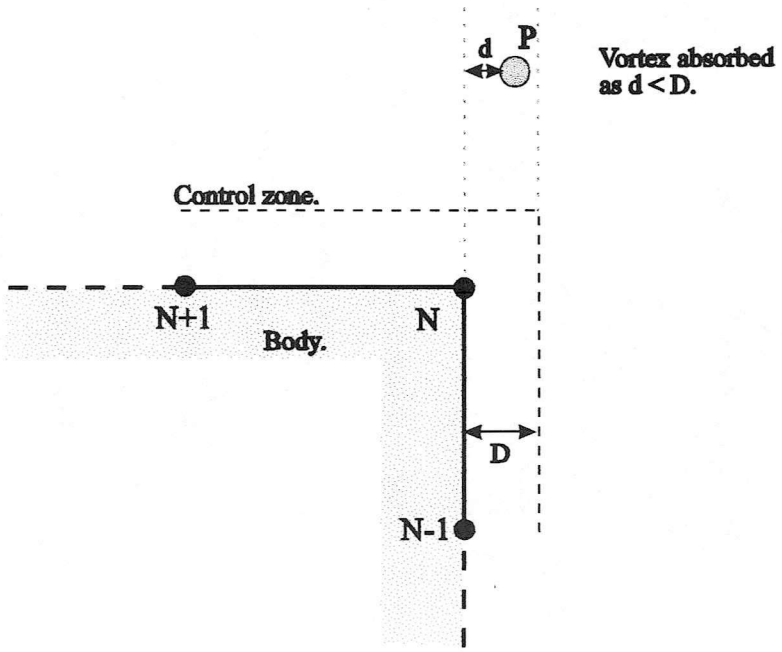

Fig. 3.2 - Problems Encountered with Absorption Check at Sharp Corners.

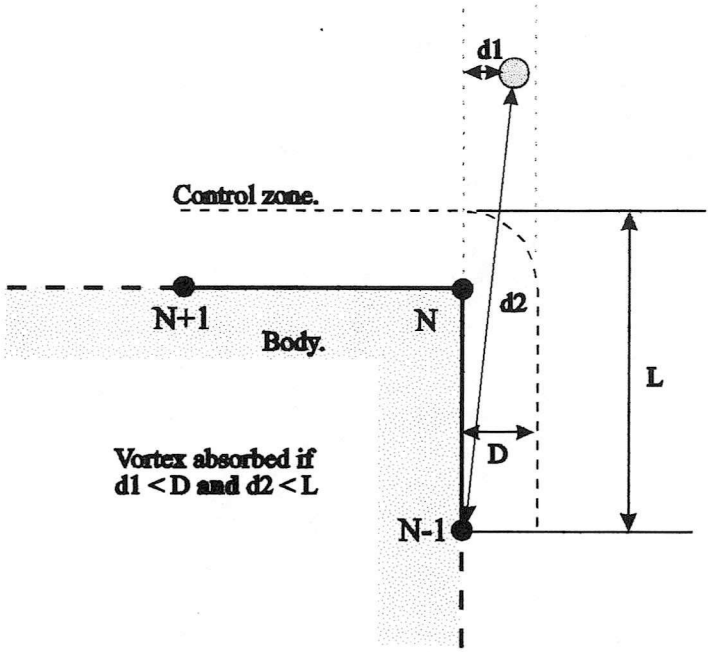

Fig. 3.3 - Modified Absorption Check to Improve Handling of Sharp Corners.

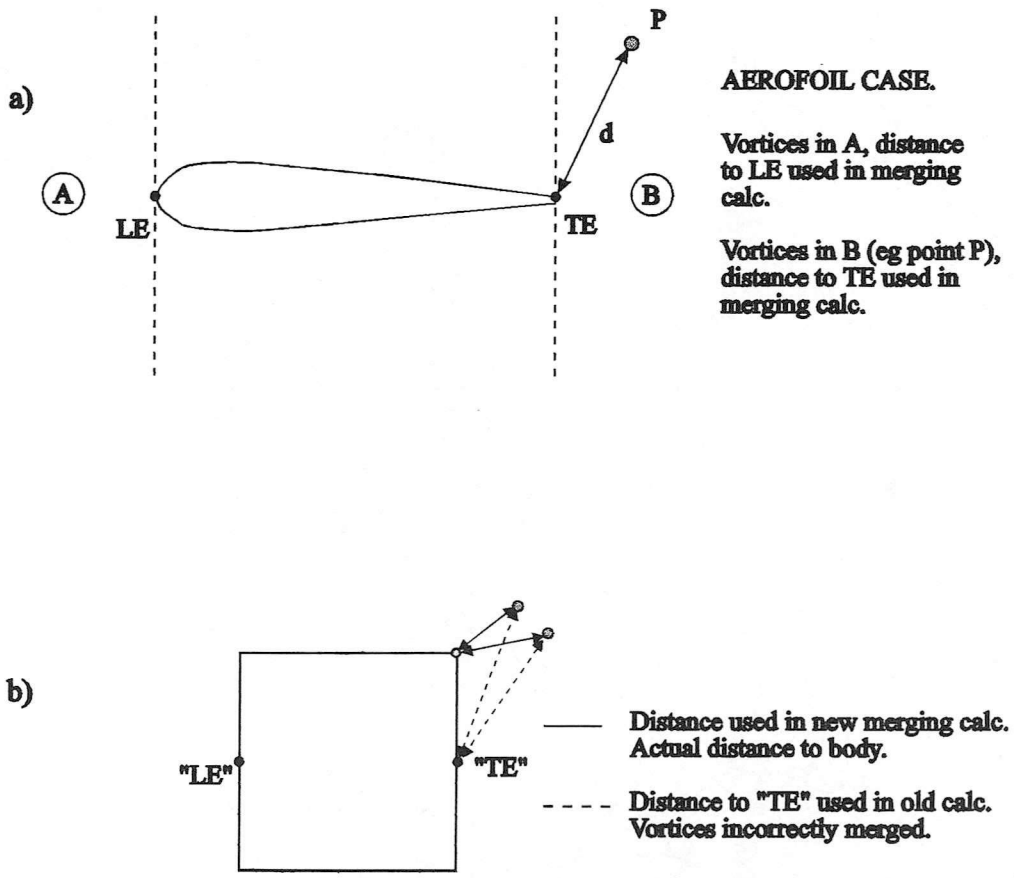

Fig. 3.4 - Modified Calculation of Distance for Merging Check.

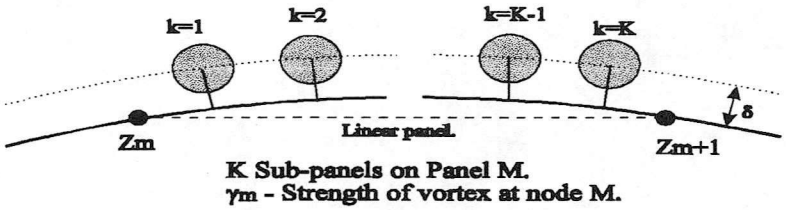

Fig 3.5 - Definition of Curved Panels.

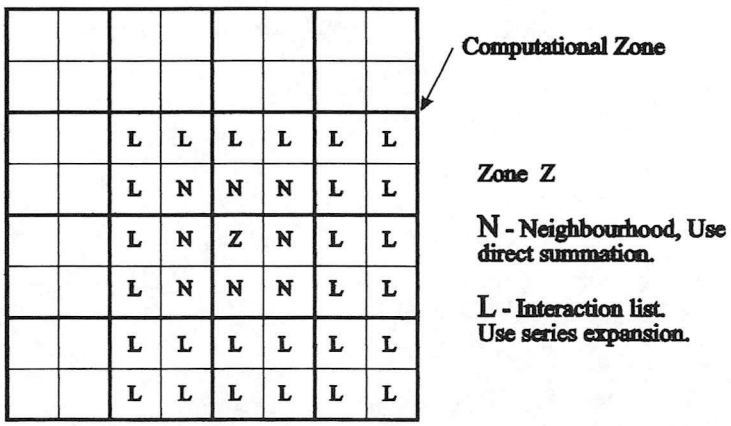

Fig. 4.1 - Zonal Decomposition : Neighbourhood and Interaction List.

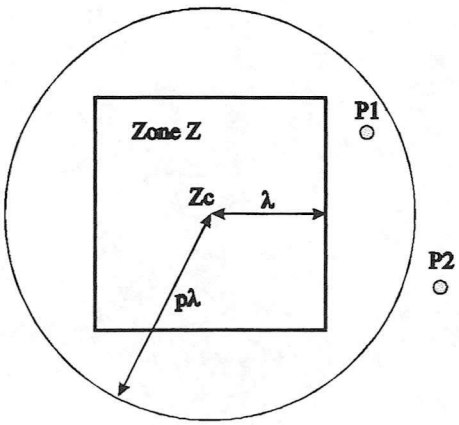

Fig 4.2 - Criteria for Using Series Expansion or Direct Summation in Velocity Calculation.

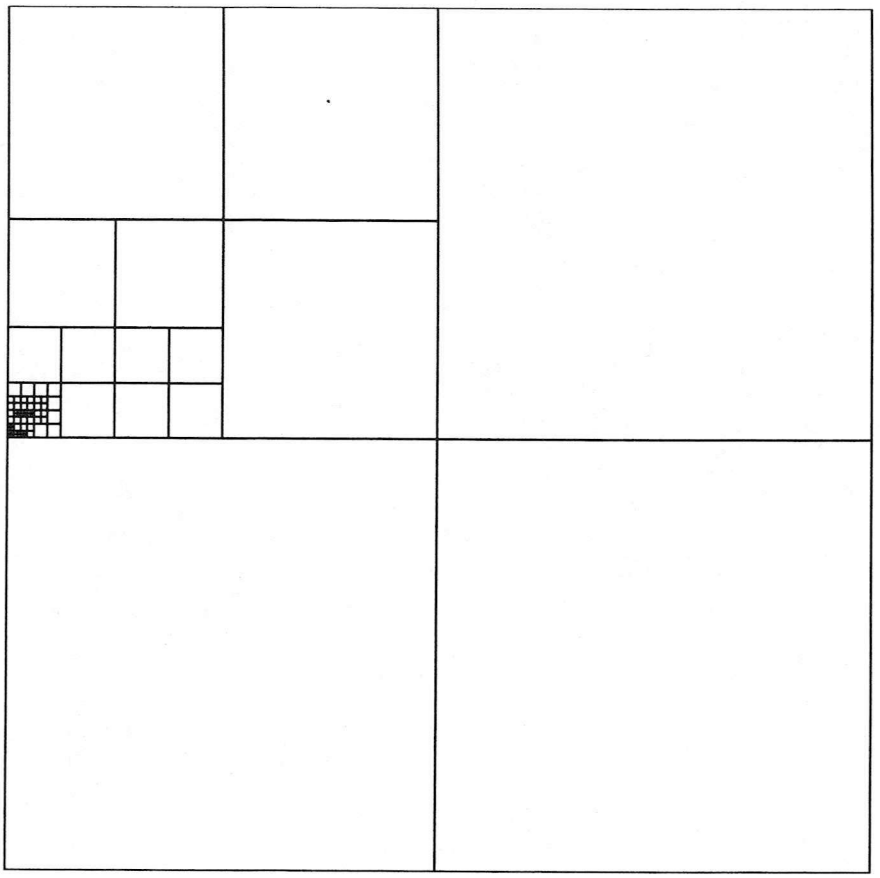

Fig. 4.3 – Zonal Decomposition for Non–Uniform Flow Field

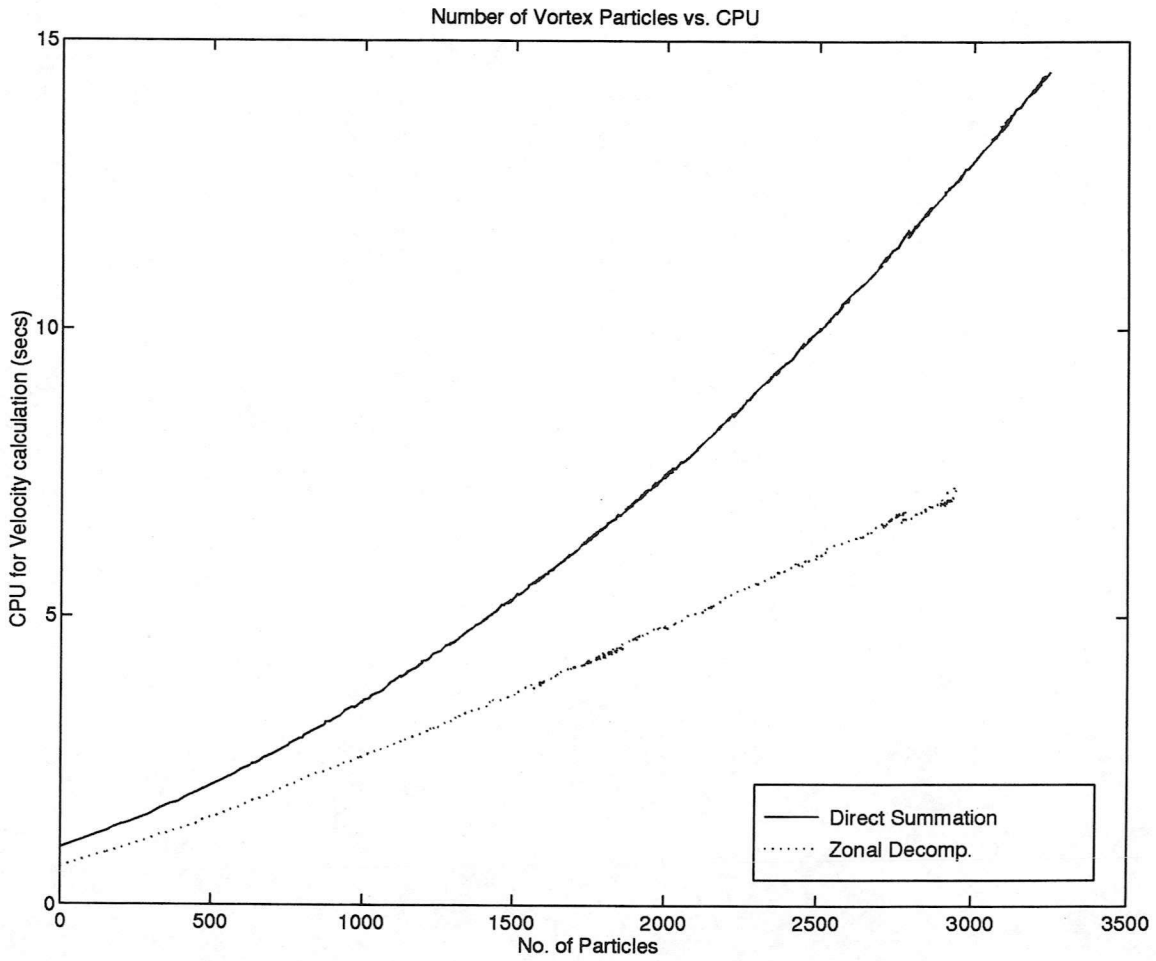

Fig 4.4 – Relationship of CPU for Velocity Calculation to Number of Vortex Particles

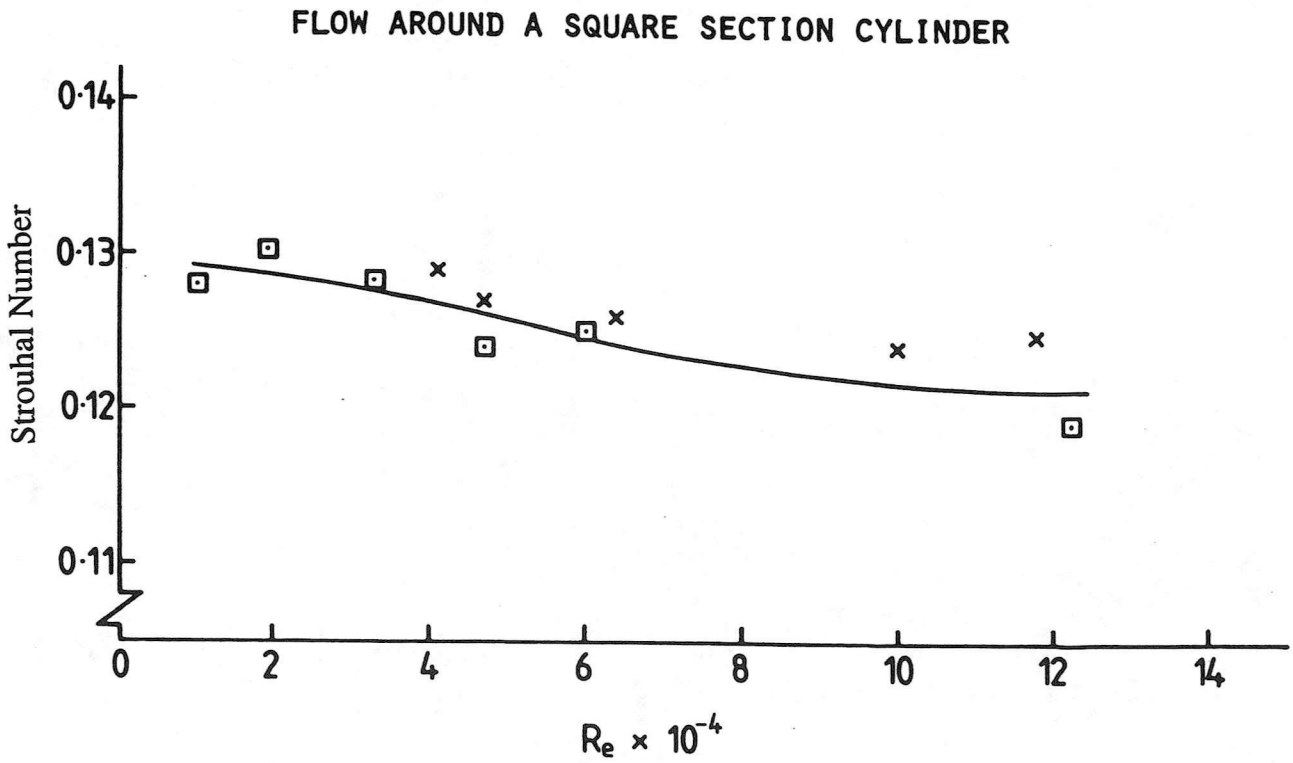

Fig. 5.1 - Variation of Strouhal Number with Reynolds Number for Square Body at 0 Degrees Incidence (OBASAJU 1983)

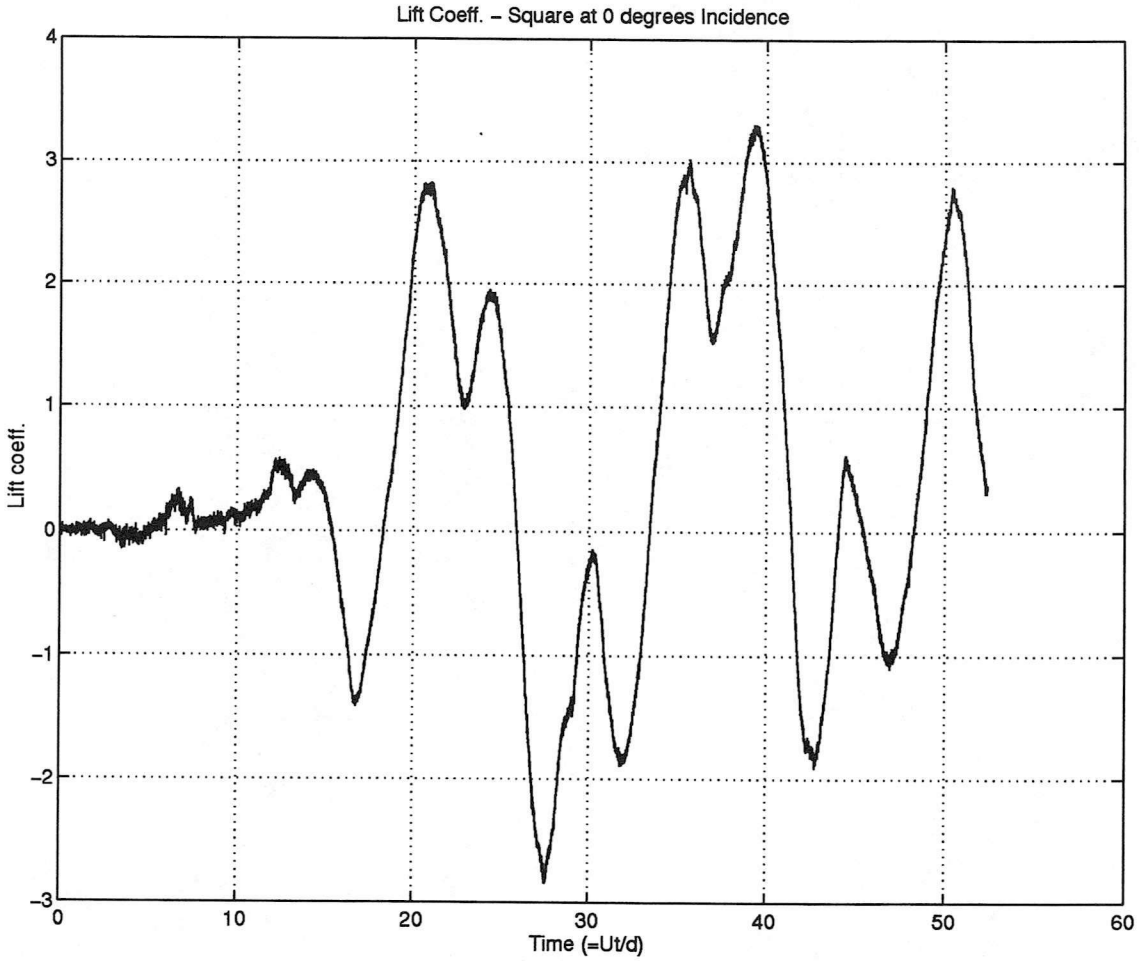

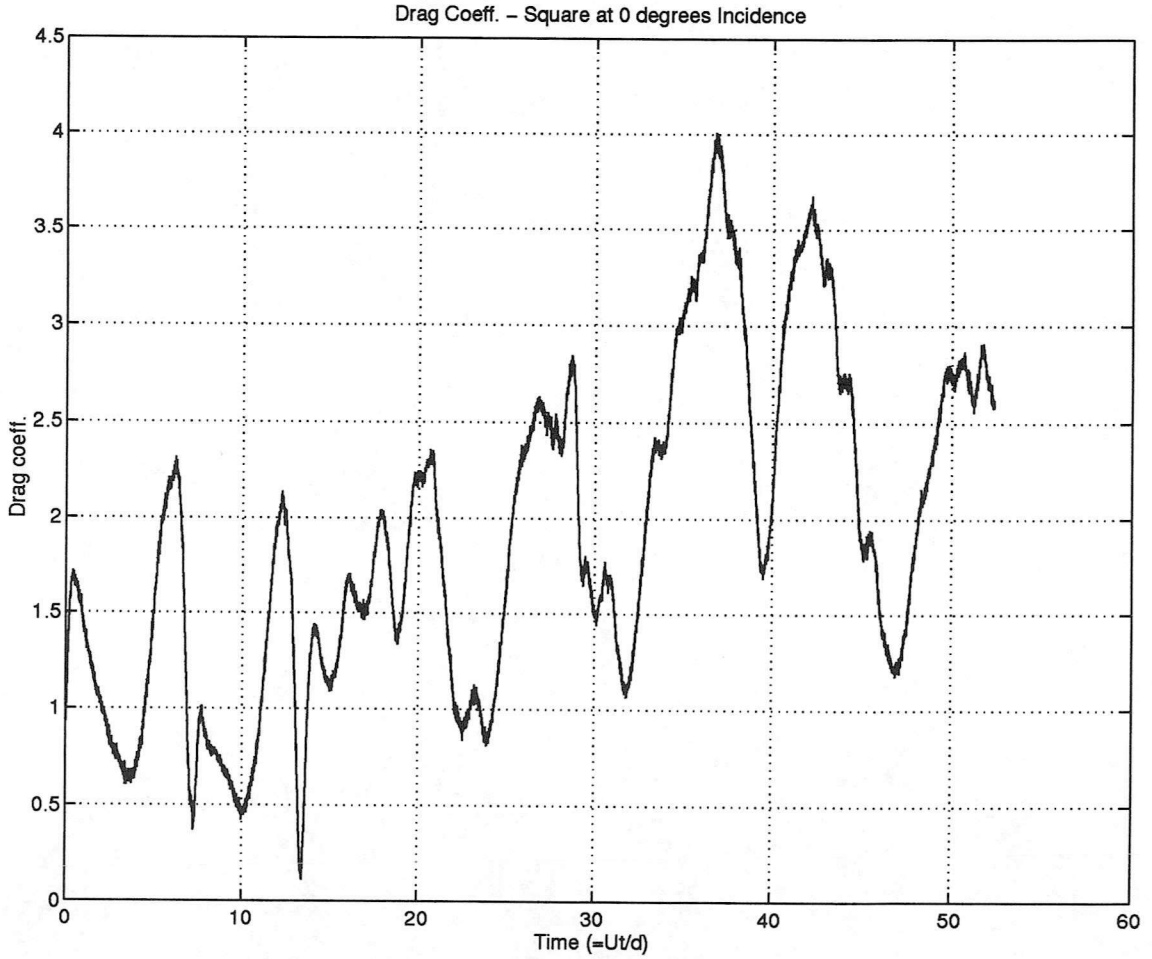

Fig. 5.2 – Lift and Drag Coefficients for Square Body at 0 Degrees Incidence.

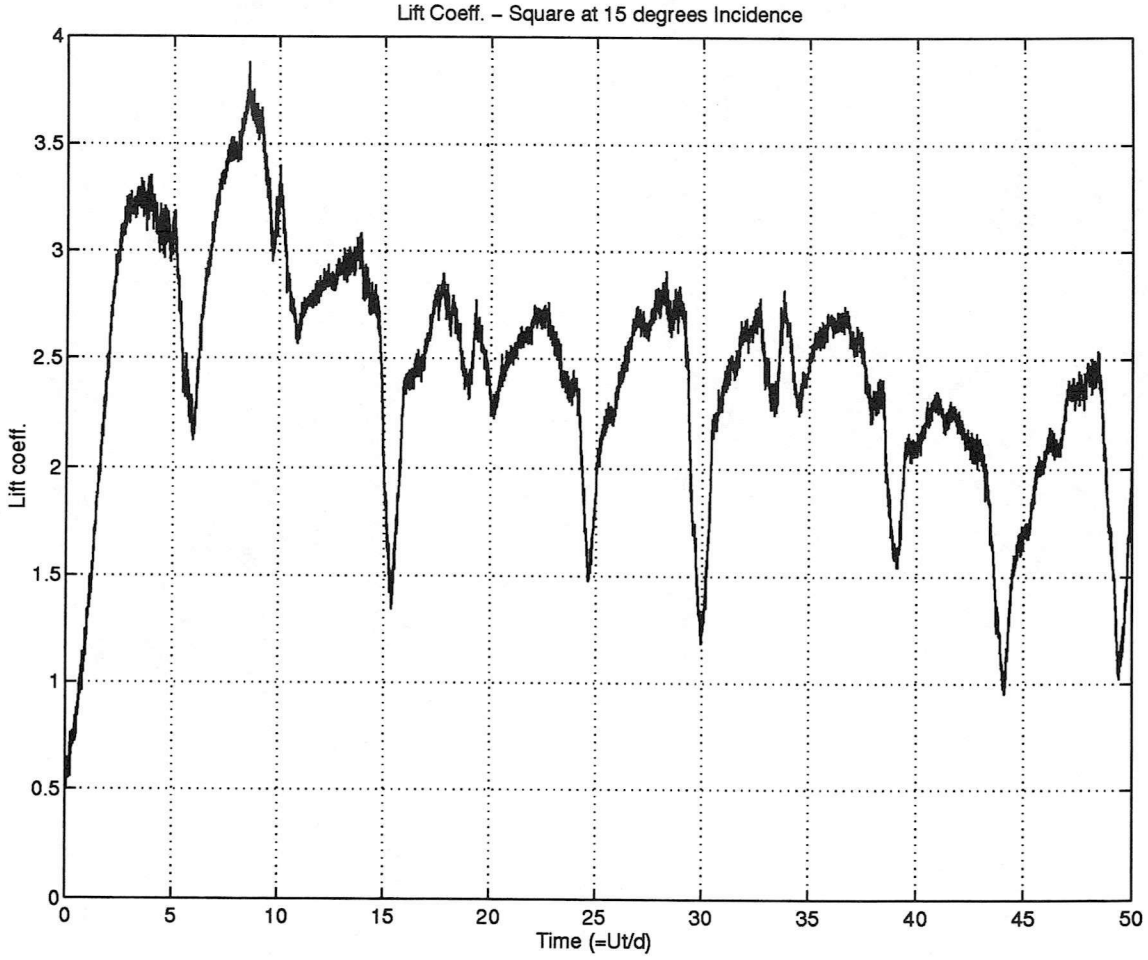

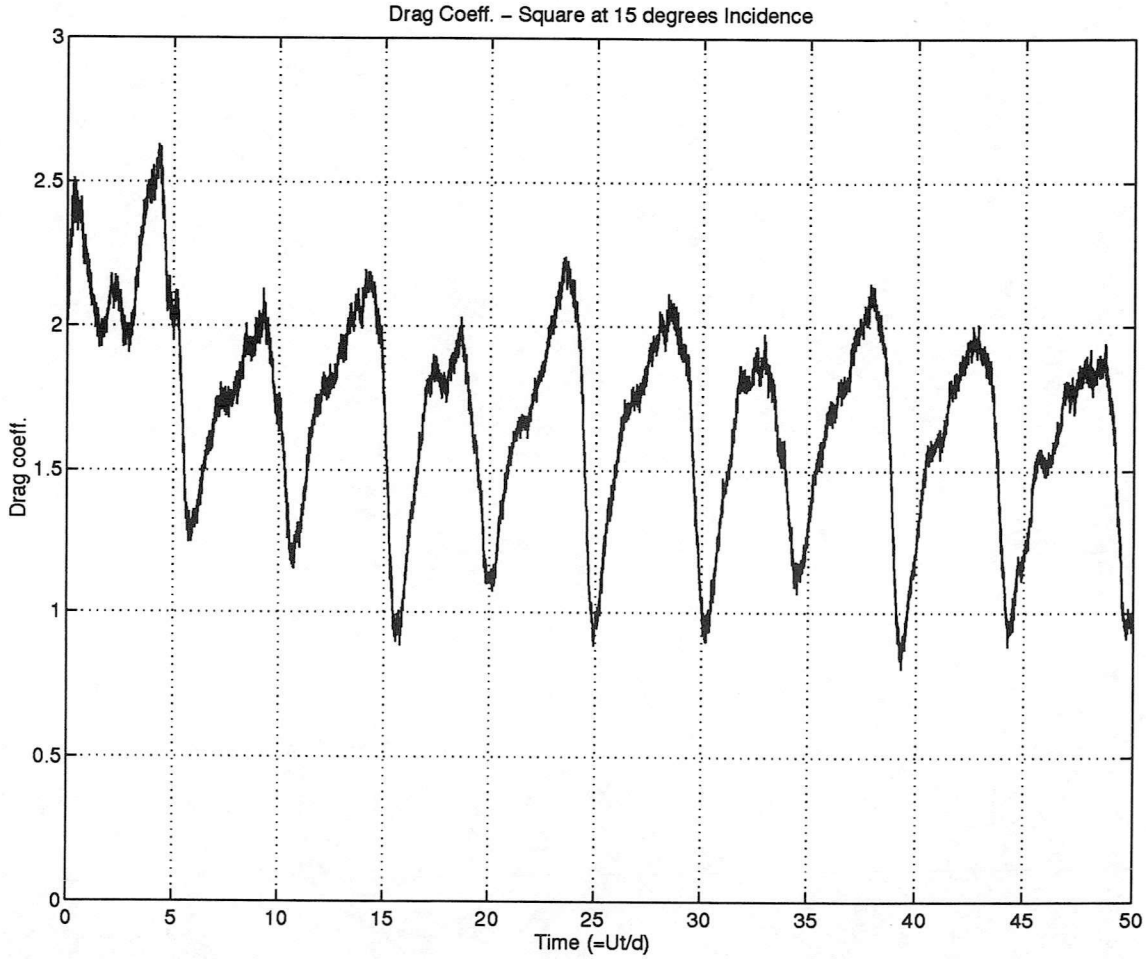

Fig. 5.3– Lift and Drag Coefficients for Square Body at 15 Degrees Incidence.

PREDICTED FLOW AROUND SQUARE BODY
AT 0 DEGREES INCIDENCE.

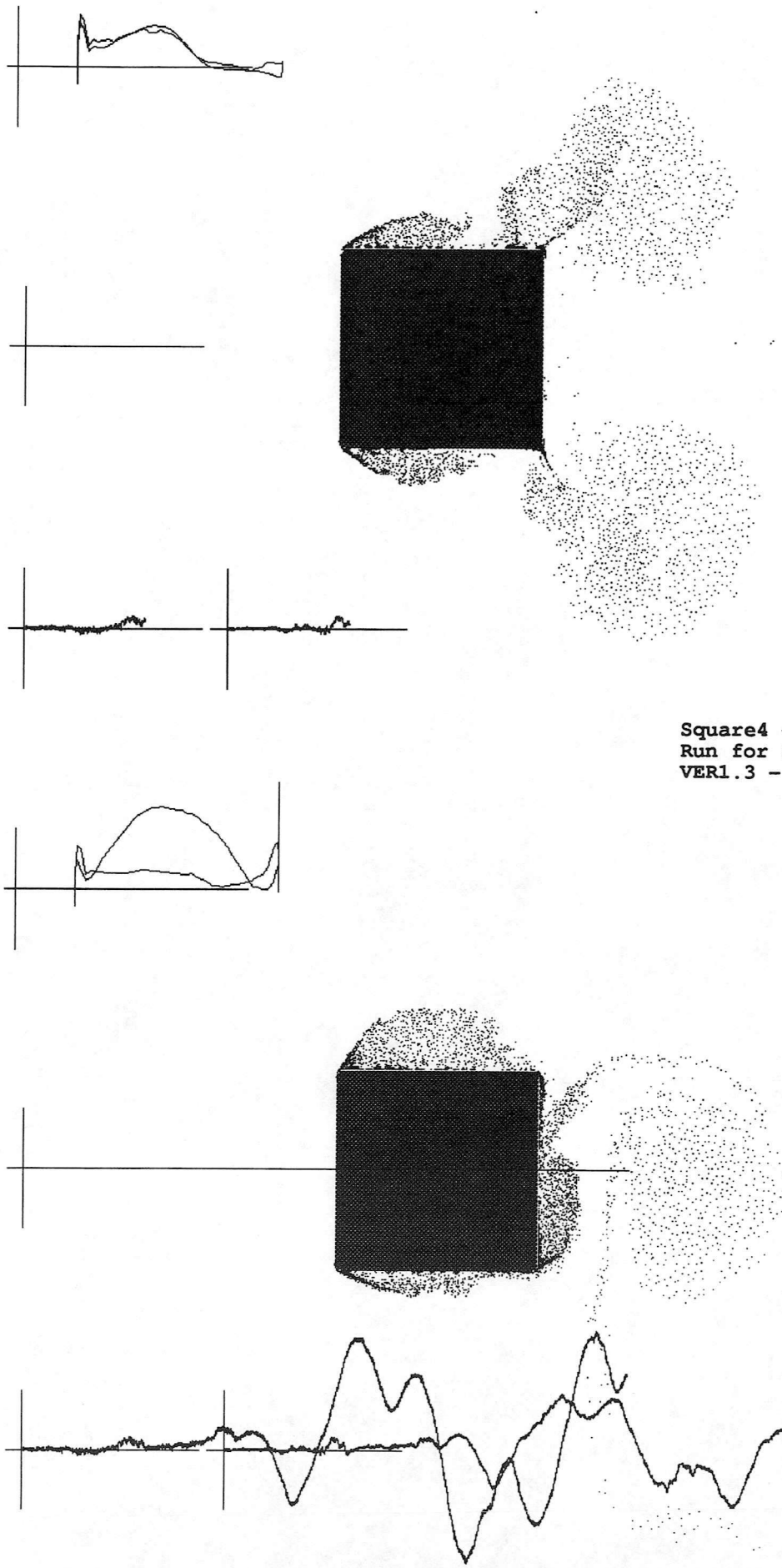

Square4 - 160 panels, 5 vortices/panel
Run for 5000 timesteps with TSTP=0.01.
VER1.3 - Square at 0 degrees incidence

Fig. 5.4 - Snapshots of Flow Field Around Square Body at 0 Degrees Incidence.

PREDICTED FLOW AROUND SQUARE BODY
AT 15 DEGREES INCIDENCE.

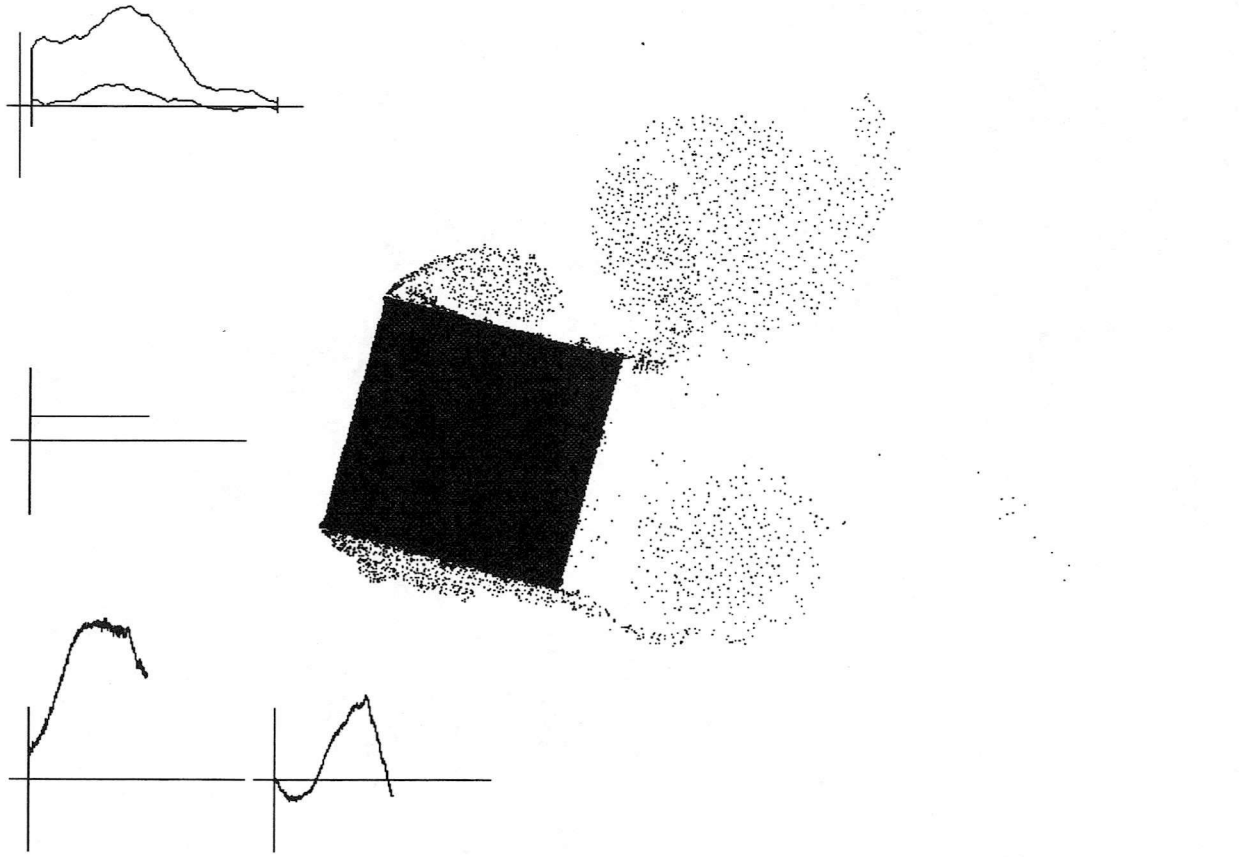

Square4 - 160 panels, 5 vortices/panel
Run for 5000 timesteps with TSTP=0.01.
VER1.3 - Square at 15 degrees incidence
NB : USING SQUARE CORNERS.

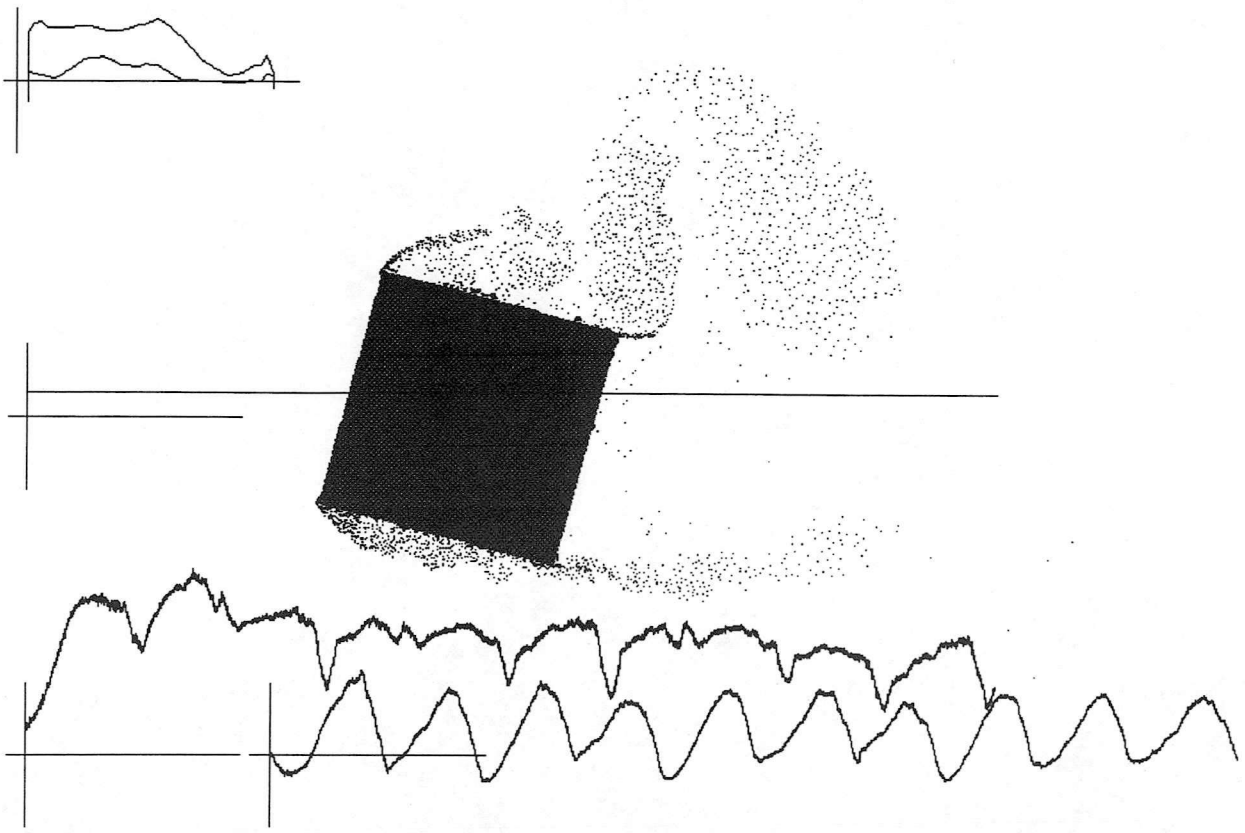

Fig. 5.5 - Snapshots of Flow Field Around Square Body at 15 Degrees Incidence.

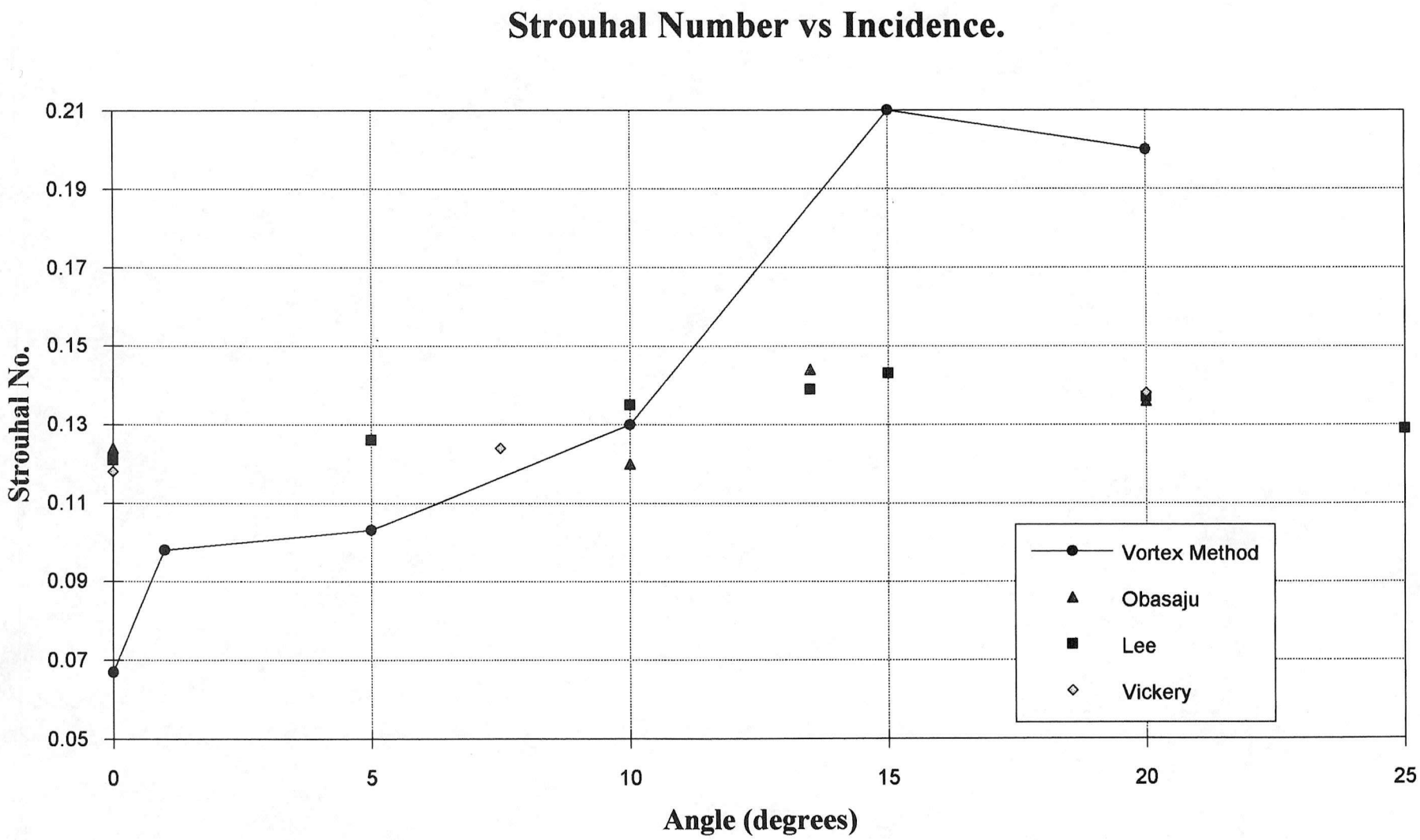

Fig. 5.6 - Strouhal Number vs. Incidence : Comparison of Predicted and Measured Data for Square Body.

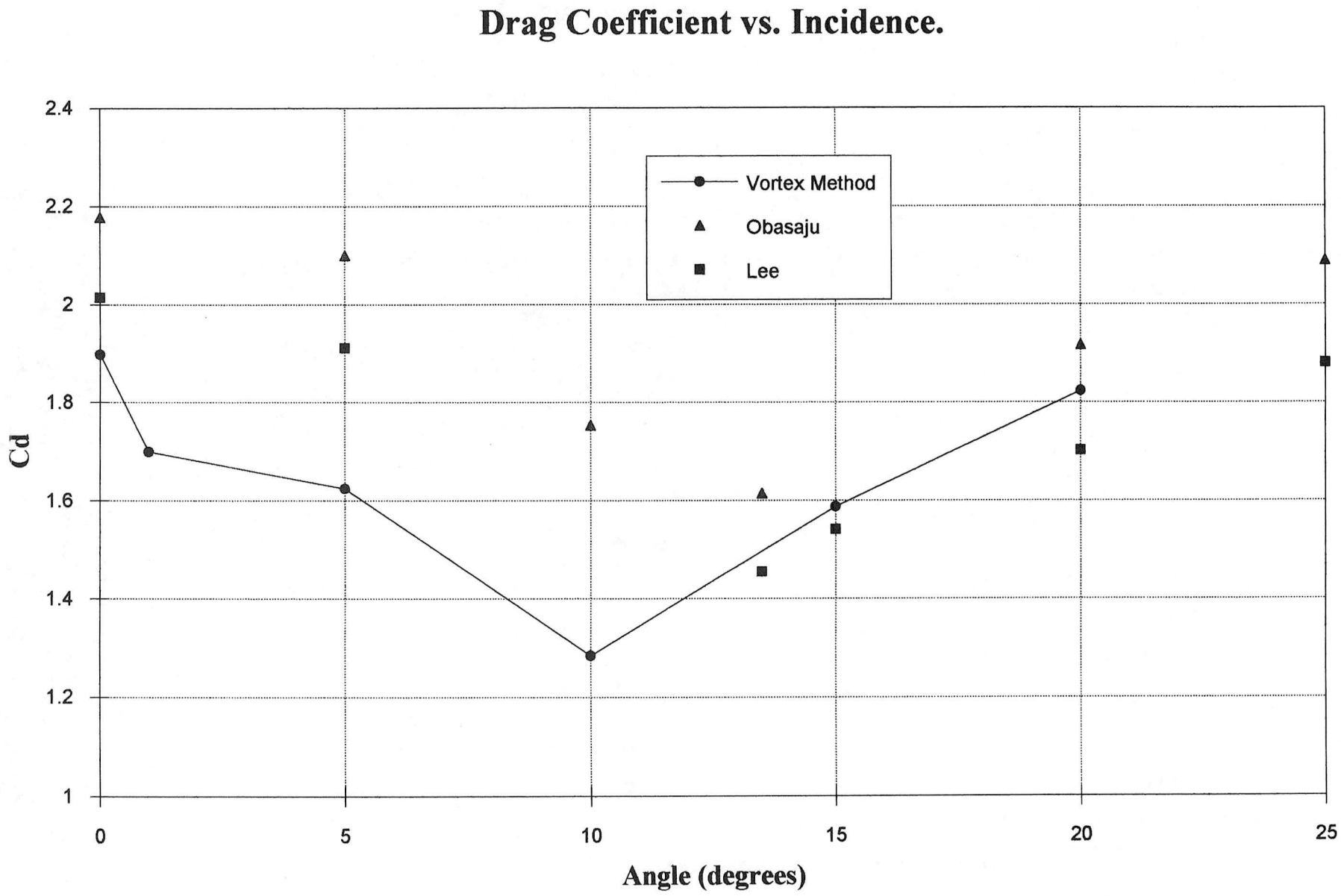

Fig. 5.7 - Drag Coefficient vs. Incidence : Comparison of Predicted and Measured Data for Square Body.

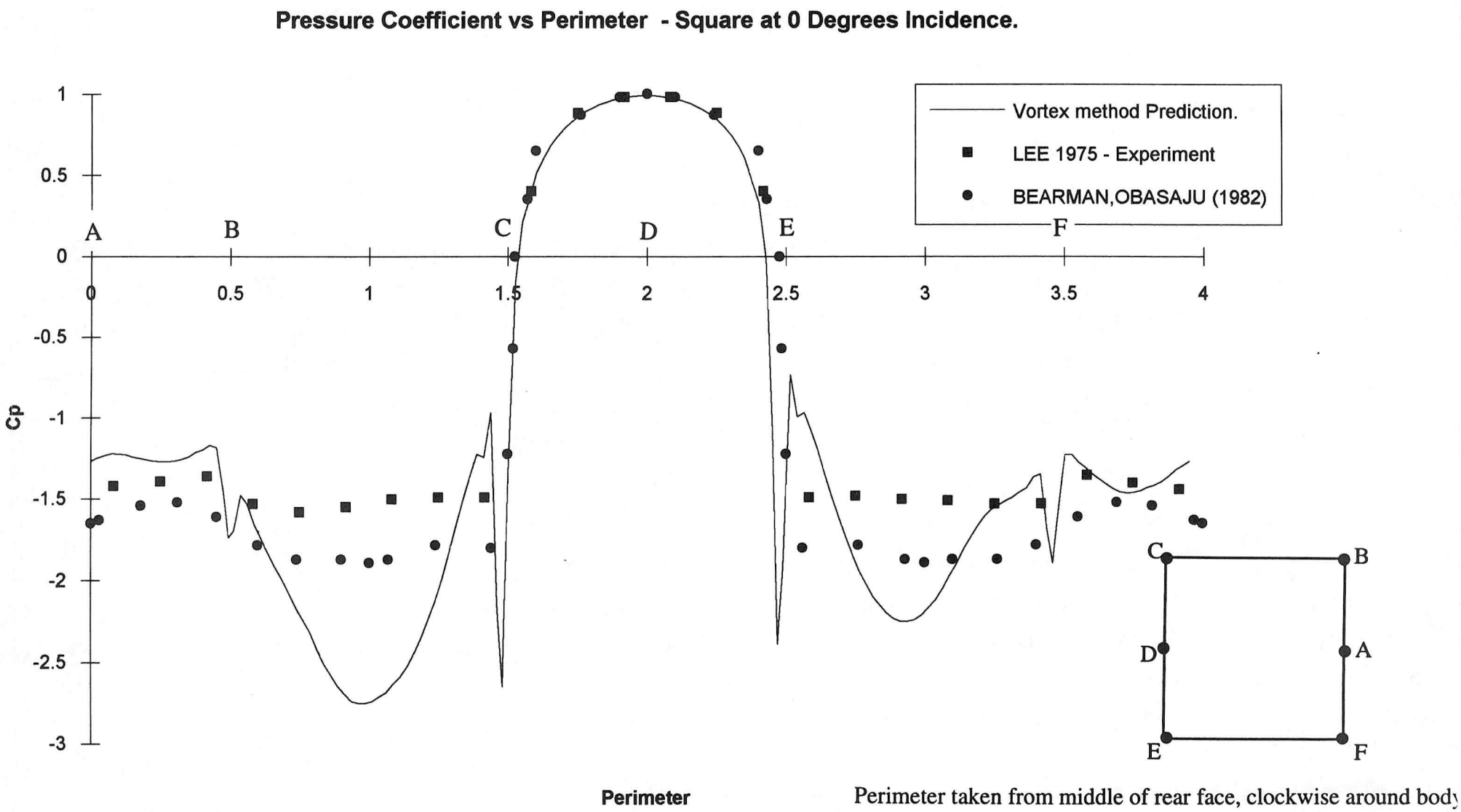

Fig. 5.8 - Comparison of Predicted Pressure Coefficient and Experimental Data for Square Body.

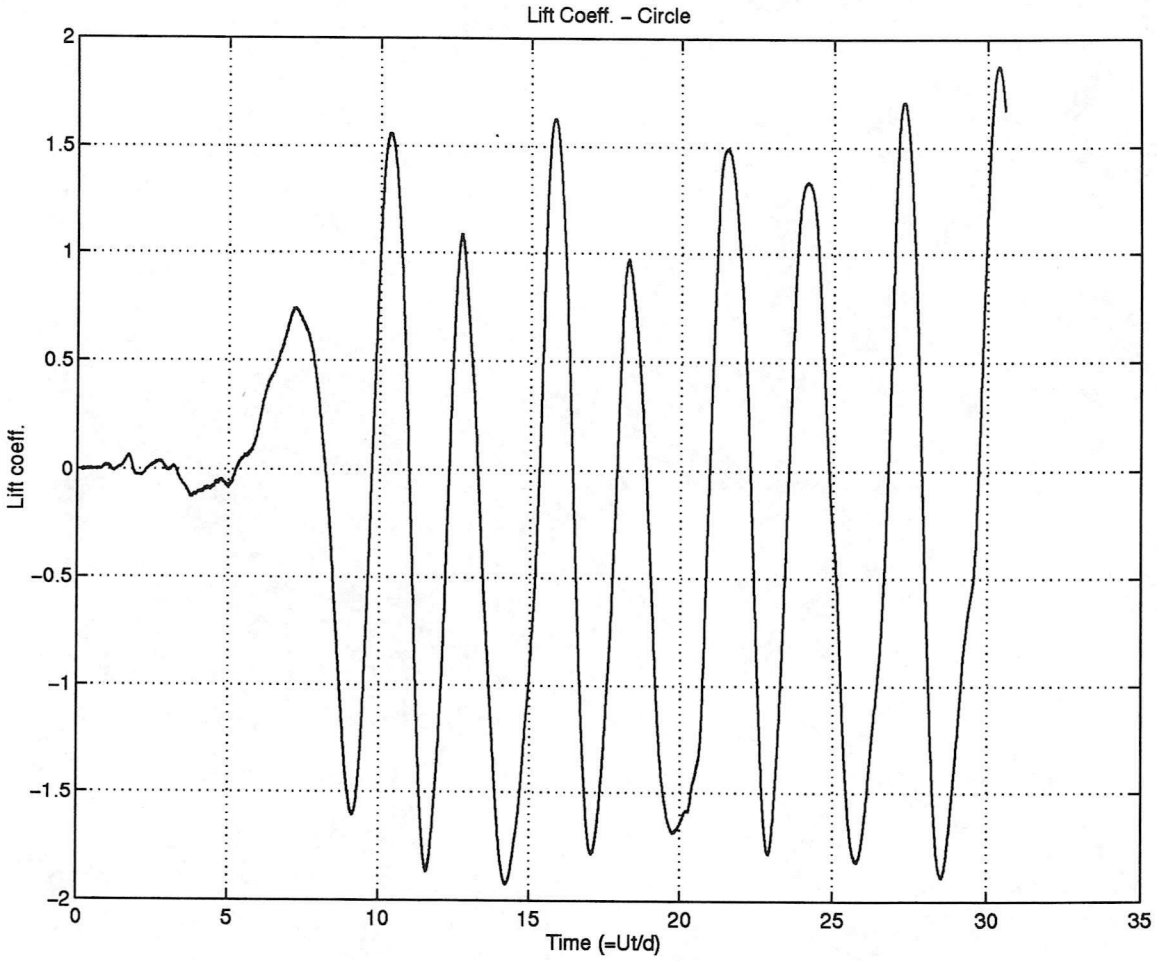

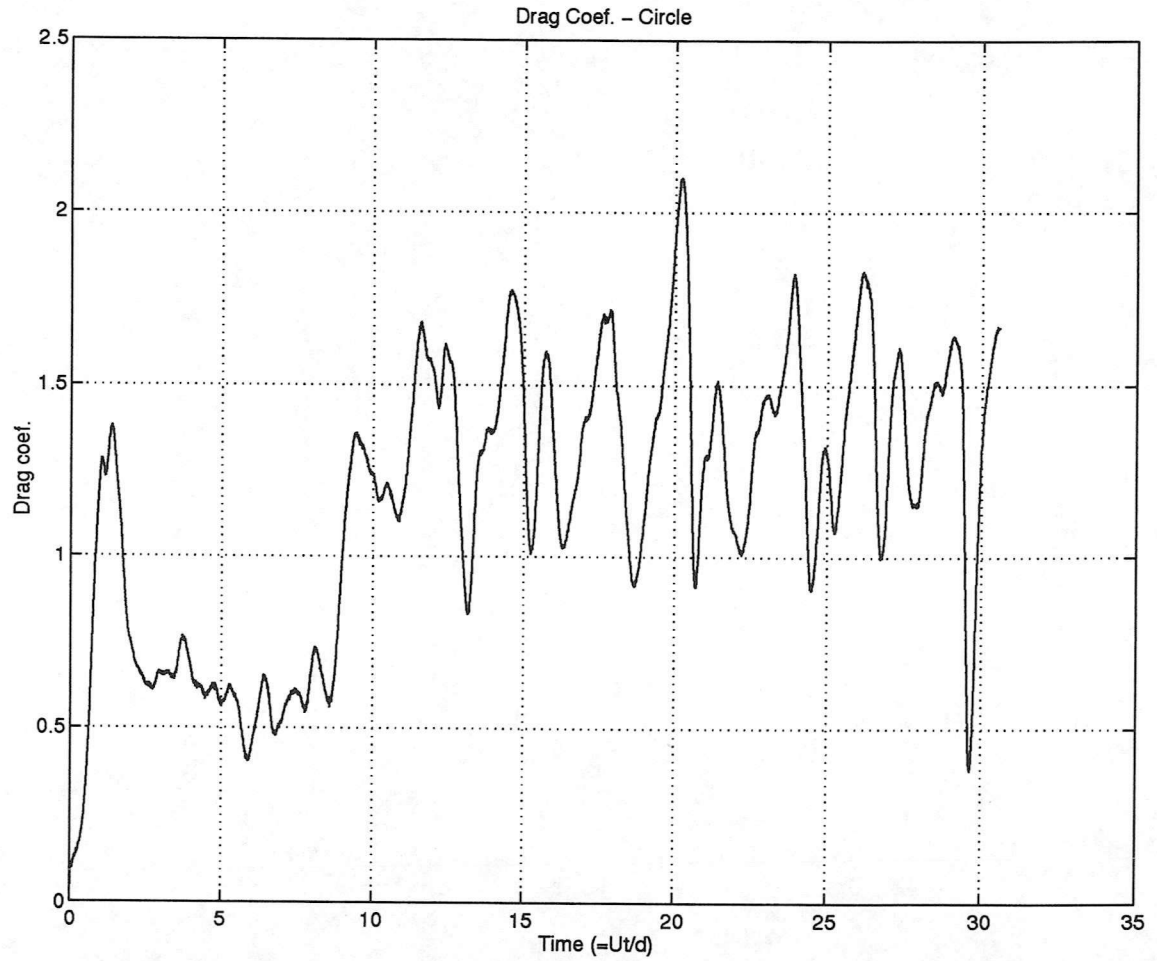

Fig. 5.9 – Lift and Drag Coefficients for Circular Body

PREDICTED FLOW FIELD AROUND
CIRCULAR BODY.

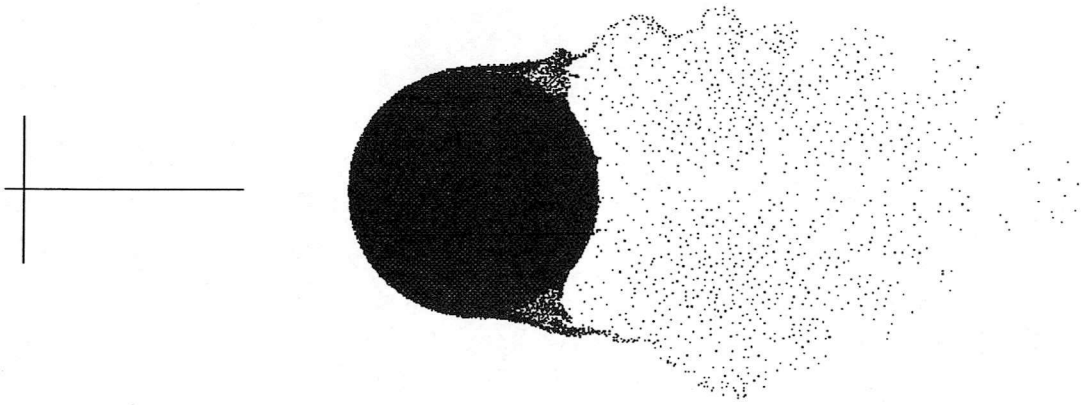

Early in Calculation.

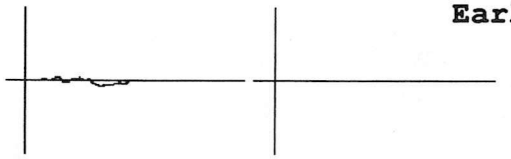

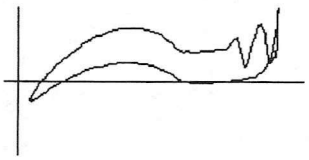

Periodic Vortex shedding later in Calculation.

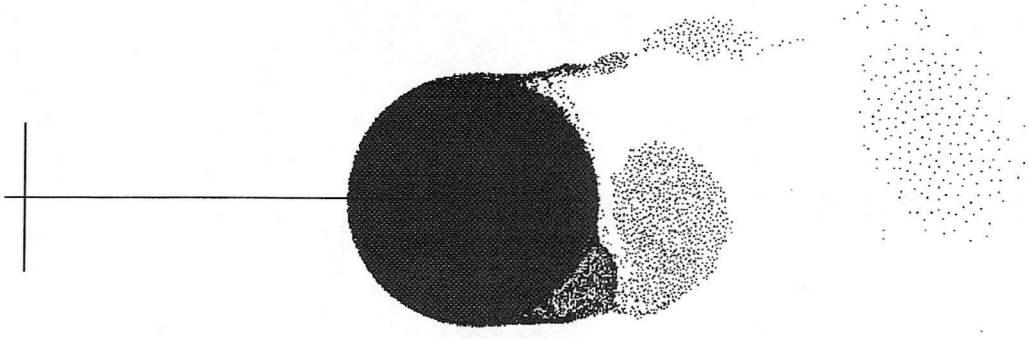

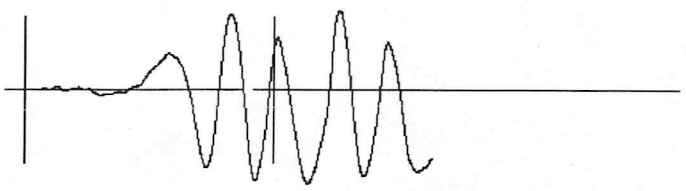

Fig. 5.10 - Snapshots of Flow field around Circle.